1 INTRODUCTION

1.1 Purpose of study

The Middle Stone Age (MSA) began in southern Africa possibly more than 200 000 years ago and ended between 30 000 and 20 000 years ago (Deacon & Deacon, 1999). The period contains key elements of change in the human species. It was during this time that key aspects of modern behaviour emerged and possibly the first anatomically modern skeletal morphology. Luminescence techniques are among the most promising methods for dating the MSA at present, and it is likely that the methods could be employed to establish an absolute chronology for the MSA. Only a handful of archaeological sites have produced luminescence chronologies (Feathers & Bush, 2000; Feathers, 2002; Jacobs *et al.,* 2003a, 2003b; Tribolo, 2003; Wadley & Jacobs, 2004). Progress towards creating reliable Optically Stimulated Luminescence (OSL) dating protocols have advanced greatly (Murray & Wintle, 2000; Jacobs, 2004; Jacobs *et al., in press.*). The key protocol used is the single aliquot regenerative (SAR) protocol (Murray & Wintle, 2000). The purpose of this study is to test the reliability of SAR protocol (by comparison between OSL and radiocarbon dates) as applied to date in South Africa in order to establish a coherent chronology for the MSA at Rose Cottage Cave (RCC).

1.2 Rose Cottage Cave

RCC is situated on the Platberg (29°13' S, 27° 28' E) near the town of Ladybrand in the eastern Free State (Wadley, 1997). It lies within the Caledon River corridor, a sub-humid, summer rainfall area about 50 km wide, that extends from the town of Clarens in the north-east to the confluence of the Orange and Caledon Rivers (Wadley *et al.,* 1992). It is located in a series of karoo sandstone hills protruding from the underlying shale (Herries & Latham, 2002). The cave is about 20 m long and 10 m wide and according to Butzer (1984a; 1984b) was formed by mechanical weathering of the sandstone strata. A large section of collapsed roof has blocked its entrance, restricting access to narrow east and

west corridors (figure 1.1). The site contains a well defined stratified sequence that extends from the Late Pleistocene (Wadley, 1997; Wadley *et al.,* 1992) in a well defined pre Howiesons Poort MSA industry (Harper, 1997; Wadley & Harper, 1989) until recent times including many of the Middle Stone Age (MSA) and Late Stone Age (LSA) industries found in southern Africa.

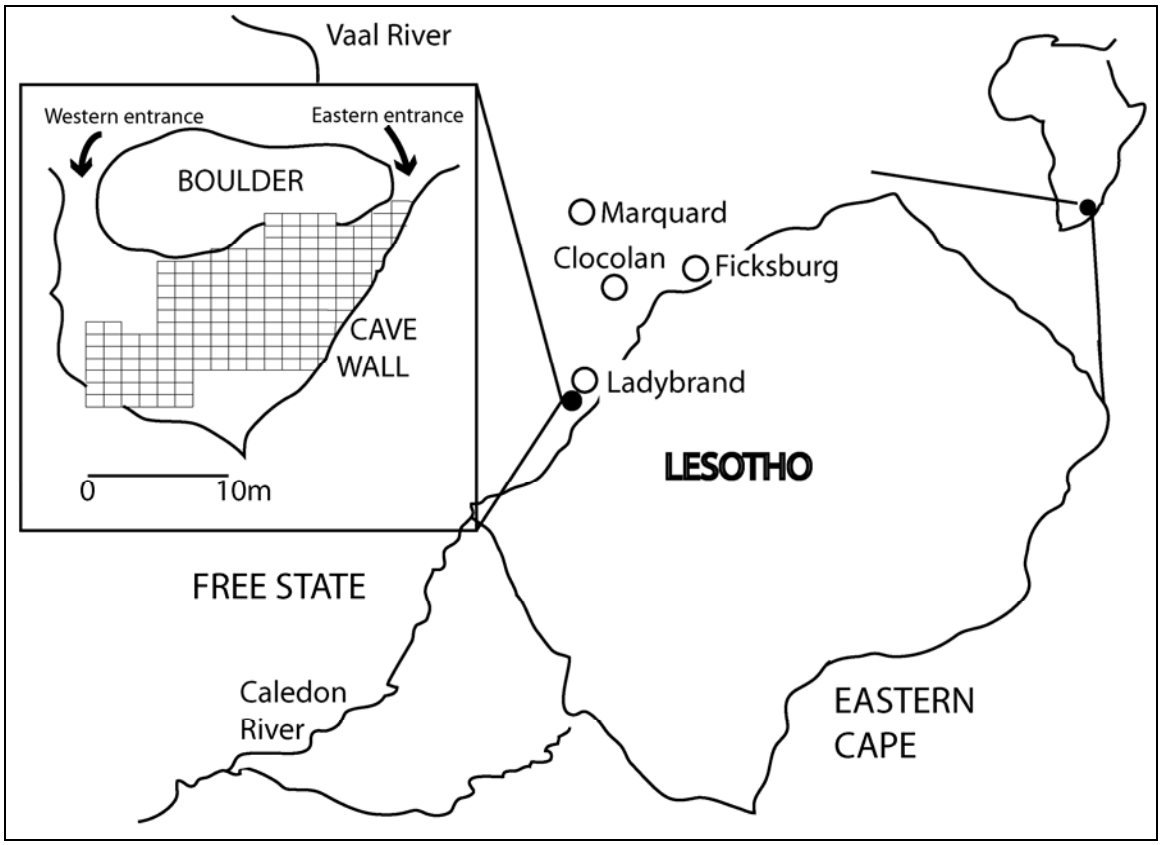

Figure 1. 1 Location of Rose Cottage Cave (modified from Wadley, 1997).

1.3 What is OSL?

OSL dating is based on the storage and release of radiation energy in crystalline mineral structures. The two principal minerals used are quartz and 'high potassium' feldspars, both of which are found in greater or lesser quantities in most sediment. The preferred mineral used to determine the age of sedimentary deposits is quartz due to a better understanding of the mechanisms of OSL production inside the crystal structure (Bøtter-Jensen *et al.,* 2003).

During the 1960s Thermoluminescence (TL) was developed at Oxford University for archaeological dating (Aitken, 1985) of pottery (Fleming, 1979). In southern Africa luminescence techniques have only recently been applied to archaeological sediments (Wintle, 1999). In 1985 the first thermoluminescence (TL) measurements were published for South Africa (Vogel, 1985). In the same year a new means of dating depositional ages was introduced by Huntley *et al.* (1985) when they introduced optically stimulated luminescence (OSL) dating using the 514 nm line from an argon laser to stimulate luminescence from quartz. The OSL technique offers an alternative method to radiocarbon dating which can be used to obtain reliable depositional ages of up to 200 000 years in the right environment (Huntley *et al.,* 1985).

1.4 Dating argument

RCC contains over six meters of deposit with a relatively even distribution of quartz and feldspar grains in most archaeological layers. The deposits at RCC consist of predominantly sandstone clast's produced through weathering or rock spalling of the cave roof and walls and laminated sediments brought in by water through faults and cracks at the rear of the cave (Butzer, 1984a, 1984b). Although the mineralogy of the sediments is well suited to OSL dating, such sediments are generally problematic due to contamination from roof and wall spalling (Fullagar *et al.,* 1996; Roberts *et al.,* 1998, 1999) and water lain sediments. Both of these mechanisms can introduce inadequately bleached grains that have the effect of changing the average OSL age of the sediment. The SAR protocol in conjunction with other checks should eliminate such contamination as well as that caused by high feldspar concentrations. Although the application of the SAR protocol in the dating of archaeological cave occupations is theoretically feasible, the approach has yet to be empirically tested. OSL dates obtained from RCC using the SAR protocol can be cross checked with known chronologies.

The most obvious test is an internal one achieved by OSL dating RCC sediments that already have a well established radiocarbon chronology. The radiocarbon chronology from RCC is one of the best in southern Africa (Butzer, 1984a;

Wadley, 1991; Wadley & Vogel, 1991), and while the true advantage of OSL dating lies in the ability to date beyond the practical limit of radiocarbon dating, some attention is given in this thesis to dating sediments with associated radiocarbon dates. For the most part the relevant radiocarbon dates conform to a regional chronology complemented by associated studies in Lesotho, particularly at Sehonghong Shelter (Mitchell, 1994). However the comparison between radiocarbon dates and OSL dates is not simple. It will become clear in the discussion on OSL dating theory that OSL dates are calculated in true calendar years, and the date is reported relative to the calendar date of the analysis. Radiocarbon dates, in contrast, are calculated relative to the year AD 1950, and the age is calculated using the Libby half-life for ^{14}C which is known to be in error by approximately 3% (Stuiver & Polach, 1977). This means that radiocarbon years are not the same as calendar years. An additional level of complexity arises from natural fluctuations in the production of ^{14}C in the atmosphere.

Both the secular variation in ^{14}C and the error resulting from the incorrect half-life used in radiocarbon dating are accommodated in the “calibration” of radiocarbon dates. In this process the measured radiocarbon date is compared with radiocarbon dates from known age tree rings in order to determine the calendar age of the sample. Recently it became clear that differences in carbon cycling in the northern and southern Hemispheres gives an approximate 40 year apparent age to the southern Hemisphere. This has to be taken into account in the calibration step for radiocarbon dates because the tree ring calibration dataset derives entirely from the northern Hemisphere. McCormac *et al.* (2004) have shown that using a fixed offset between the northern and southern hemisphere is erroneous and calibration of the southern hemisphere is therefore best achieved on dendro-chronologically dated wood. Unfortunately no such dataset exist for the southern hemisphere for the period before 1000 years ago. Furthermore, the calibration record between 26 ka and 50 ka is constructed from a variety of datasets such as laminated lake sediments, corals and speleothems. Van der Plicht *et al.* (2004) have noted that offsets greater than 2000 years exist between these datasets and recommend that this period should not be used in radiocarbon calibration.

The RCC radiocarbon dates in this study were calibrated using the Southern Hemisphere 1998 calibration dataset (SH98) (Stuiver *et al.,* 1998a). It should be noted that this dataset is interpolated on relatively few measurements (Talma & Vogel, 1992, 1993) combined with a average 40 year offset from the northern hemisphere 1998 dataset (INTACAL 98) (Stuiver *et al.,* 1998b).

The calibration issues around radiocarbon are complex and they result in several different representations of the dates. The radiocarbon dates are initially reported as dates “BP” or Before Present which is defined as the year AD 1950. After calibration the date is presented in the form of Julian Calendar years AD or BC. In order to compare these dates with OSL dates it is necessary to consider AD calibrated radiocarbon dates as negative, BC calibrated radiocarbon dates as positive, and to add to this the year in which the OSL date was determined.

Another test of the OSL approach is to compare the dates from RCC with those from other sites derived using other methods, or even using OSL methods under different circumstances. RCC is one of only seven known MSA sites to contain a well stratified Howiesons Poort (HP) assemblage (Wadley, 1997; Harper, 1997; Wadley & Harper, 1989) that can be cross-checked by an emerging HP chronology based on other archaeological sites shown in figure 1.2.

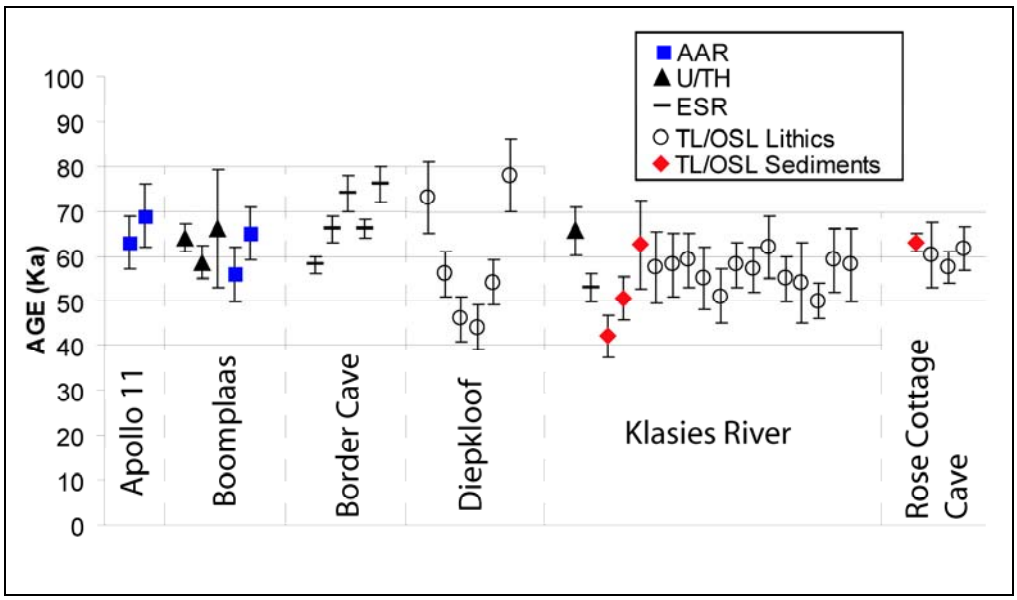

Figure 1. 2 Different ages of the Howiesons Poort. The general consensus age occurs between 50 Ka and 70 Ka. (Tribolo, 2003; Feathers, 2002; Grün & Beaumont, 2001; Vogel, 2000; Miller *et al.,* 1999; Grün *et al.,* 1990; Murray pers. comm.).

1.5 Importance of study

The development of chronometric dating techniques in recent years has helped to establish absolute chronologies and re-construct paleo-climates. If it can be shown that OSL dating, using the SAR protocol, can establish a coherent MSA chronology at RCC, especially for the HP, then it will be possible to illustrate the link between technological adaptation and changing environments. This would aid development of archaeological and evolutionary thinking, as well as prove the reliability of previous OSL results. If on the other hand it is found that the SAR protocol cannot be used reliably at RCC, the problems need to be identified, and an alternative dating protocol needs to be applied to RCC and OSL dates obtained at other archaeological sites.

A more specific issue that needs to be addressed is the chronology of the MSA/LSA transition. At Border Cave (BC) Beaumont defines the Early Later Stone Age (ELSA) and he also classified the pre-Robberg levels at RCC as ELSA (Beaumont 1978). Wadley (1991) and Wadley & Vogel (1991) argue that the RCC layers predating 26 900 +-550 (Pta 6303) (uncalibrated BP) (Layers stratified below and including layer Ruth) are typologically MSA in nature. This implies that Beaumont's ELSA classification is too broad and it includes both the terminal MSA and the MSA/LSA transition assemblages. To some extent this argument is typological, but it is essential that similar age assemblages be compared between RCC and BC. The relevant BC assemblage derives from a layer known as the 1WA that has been subsequently dated to 38.5 ka (uncalibrated BP) (Bird *et al.,* 2003). In the same way that the OSL dates provide an independent chronology for the pre-26 000 year old deposits (i.e. for the layers in which radiocarbon calibration becomes problematic), so too the Electron Spin Resonance dates for BC provide an independent chronology for this site. The ELSA at BC is placed between 41 ka and 30 ka (calibrated relative to AD 2001) (Grün & Beaumont, 2001). The key contribution in this study is to identify the corresponding age layers at RCC in order that a direct comparison can be made between the relevant stone tool assemblages.

Detailed explanations of OSL theory is explained in the course of this study. These explanations are divided into two sections the first focuses on the numerator in the OSL age equation, including the equipment that is used and, the second focuses on the denominator in the OSL age equation. These two aspects are analysed separately in this thesis and brought together in the final chapter. The calculations in the final chapter uses the most probable values in the OSL age equation and are then compared to an existing radiocarbon age chronology for RCC.

2 ROSE COTTAGE CAVE

2.1 General Background

The first excavations at RCC were conducted under the supervision of B. D. Malan, a former student of A. J. H. Goodwin in the 1940s (Malan, 1952). From 1943 till 1946 he excavated RCC in what was probably the longest excavation in South African archaeology at the time (Mason, 1989). The primary aims of his excavations were:

- To ascertain the cultural stratigraphy of the Free State Wilton and Modderpoort cultures
- To study the MSA/LSA transition
- To establish the relationship between the various phases of rock art represented on the cave wall.

In the 1920s South African archaeology had broken away from European stone tool typological nomenclature largely due to the work of A.J.H. Goodwin and C. Van Riet Lowe (Goodwin & Van Riet Lowe, 1929; Goodwin, 1935). In 1929 the term Middle Stone Age (MSA) had been adopted due to the emerging variability in the Early Stone Age (ESA) and Later Stone Age (LSA) and it had been interpreted as a 'Mousterian' influence that had diffused into southern Africa. The MSA was characterised by the Levallois technique and broadly defined by Goodwin & Van Riet Lowe (1929) as a flake tool industry. The Howiesons Poort (HP) MSA sub-stage was seen as similar to the Magosian and by 1947 was accepted by the Pan African Congress on Prehistory, as the final phase of the MSA (Malan, 1952).

It was in this context that Malan divided the RCC sequence into a Modderpoort industry (basal layers), which he classified as a sub unit of the 'South African Magosian'. This was followed by about 2.1m of almost sterile sand topped by 1.7m of 'grey ash' near the top of the sequence which he associated with the LSA (Malan, 1952). Without the aid of absolute dating, the 'Magosian' material from RCC seemed an ideal candidate for a MSA/LSA

transitional industry. Malan subsequently became influential in extending the term ‘Magosian’ to the rest of southern Africa. Hoffman, one of Malan’s associates, classified the levels above the ‘Magosian’ (Howiesons Poort levels) into three different ‘cultures’. From base to top these were termed the ‘Koning culture’ (MSA IV), an unnamed blade culture and a Wilton industry (Wadley, 1991). Breuil (Wadley, 1991) identified the unnamed blade culture as a unique assemblage that could represent a new stone tool industry in southern Africa. Later excavations would confirm that Breuil had identified the first occurrence of the Robberg industry in South Africa (Wadley, 1991).

Prior to the 1950s the MSA was thought to begin around 4000 years ago followed by the LSA 2000 years later (Goodwin & Van Riet Lowe, 1929). By the mid 1950s the three age classification scheme (ESA, MSA, LSA) expanded to include the First and Second Intermediate stages (Deacon, 1990). The Magosian became the second intermediate phase. This was due to a paradigm shift that recognised the environment as a driver of cultural change. A great contribution to this paradigm came from the work of J. D. Clark in his synthesis ‘*The prehistory of southern Africa*’ (1959). Central to Clark’s work was the notion of Climato-stratigraphic dating, a relative dating technique based on the ‘Pluvial Hypothesis’ (Leakey & Solomon, 1929) in which the advance and retreat of alpine glaciers could be used as climatic indicators. In Africa, pluvial succession was proposed on Rift Valley lake deposition (Deacon, 1983) and the entire MSA was placed within a period of increased rainfall called the Gamblian Pluvial, the equivalent of the Würm Glacial in Europe (Clark, 1959).

The advent of radiocarbon dating of archaeological sites (Libby *et al.,* 1949) had a profound effect on South African archaeology. The first proposed ^{14}C chronology for southern Africa (Clark, 1959) provided a ^{14}C date of 60 000 B.P. from an Acheulian level (ESA) at Kalambo Falls, Zambia (Clark, 1969) and suggested that the MSA lasted between 38 000 BP and 6000 BP, while the LSA post-dated 6000 BP. In 1962 P. B. Beaumont, who was working under R. J. Mason at the time, re-excavated RCC with the specific aim of collecting charcoal samples for dating (Wadley, 1991). Several ^{14}C dates were

obtained by Beaumont from the LSA layers. He also collected material from the almost sterile sands that produced infinite dates of greater than 50 000 years and confirmed for the first time the real antiquity of the cave deposits (Butzer 1984b; Mason, 1962, 1969, 1989; Wadley & Vogel 1991; Wadley, 1991).

In 1972 a revised ^{14}C chronology for southern Africa was published (Vogel & Beaumont, 1972a, 1972b) that suggested that the MSA probably lasted between 100 000 years ago and 35 000 years ago. This framework was later augmented by palaeo-environmental reconstruction based on evidence emerging from other MSA sites. At RCC, Beaumont introduced a new industrial term which he called the Early Later Stone Age (ELSA). His RCC sequence was grouped into the Magosian followed by the ELSA and topped by a three phase Wilton and 'Pre-Wilton' industry in the upper ash layers (Wadley & Vogel, 1991). He recognised Hoffman's unnamed blade culture to be representative of a Robberg-like Industry which he grouped along with the 'Koning culture' and Malan's final MSA into the ELSA (Beaumont, 1978).

In the late 1970s and early 1980s, K. W Butzer visited RCC and collected further ^{14}C samples (Wadley & Vogel, 1991; Butzer, 1984b) from both the LSA and MSA levels of Malan and Beaumont's excavations. The ages he obtained were associated with material classified according to Beaumont's scheme. The main purpose of Butzer's visit however, was not to try and resolve a chronological framework for the stone age, but rather to study the processes of sedimentary deposition (Butzer, 1984a; 1984b; Wadley, 1991). Butzer (1984a, 1984b) recognized the climatic implications of the RCC sedimentology, and interpreted the well-laminated water-lain sediments to be a result of heavy and protracted rains, while silt and clay-sized grains indicate lower rainfall (Herries & Latham, 2002). His environmental model at RCC is controversial and does not correlate to other environmental studies performed at the site (Wadley, 1997).

In 1987 new excavations started at RCC under L. Wadley, who excavated through the LSA to the top of the sterile sands (Wadley, 1991, 1995, 1996,

1997). P. T Harper excavated through exposed MSA sections left after the Malan and Beaumont excavations (Harper, 1997; Wadley, 1997). The work by Wadley and her team produced a coherent well-defined LSA sequence. The Wadley excavations lasted from 1987 till 1997 and focused primarily on the spatial analyses of the occupation levels and reconstruction of past environments (Avery, 1997; Engela, 1995; Esterhuysen, 1996; Esterhuysen & Smith, 2003; Herries & Latham, 2002; Plug & Engela, 1992; Scott, 1989; Wadley *et al.,* 1992). Figure 2.1 depicts the spatial orientation of RCC showing the major excavated areas and Figure 2.2 shows the development of the lithostratigraphic sequence from 1943 till Wadley's excavation.

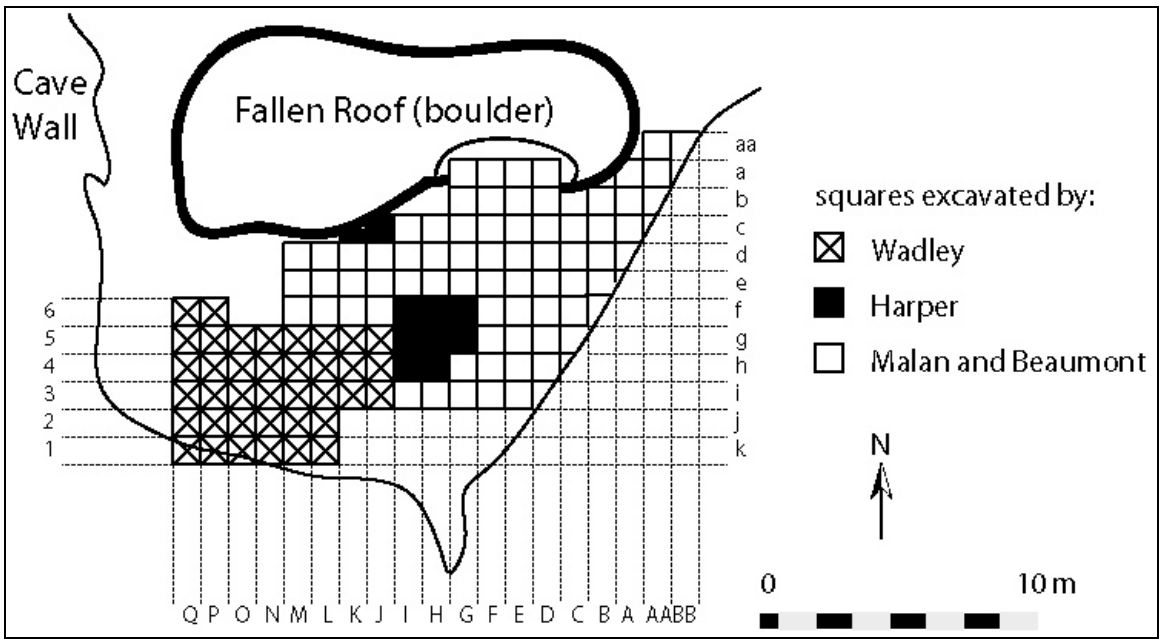

Figure 2. 1 Plan of Rose Cottage Cave after Wadley 1997

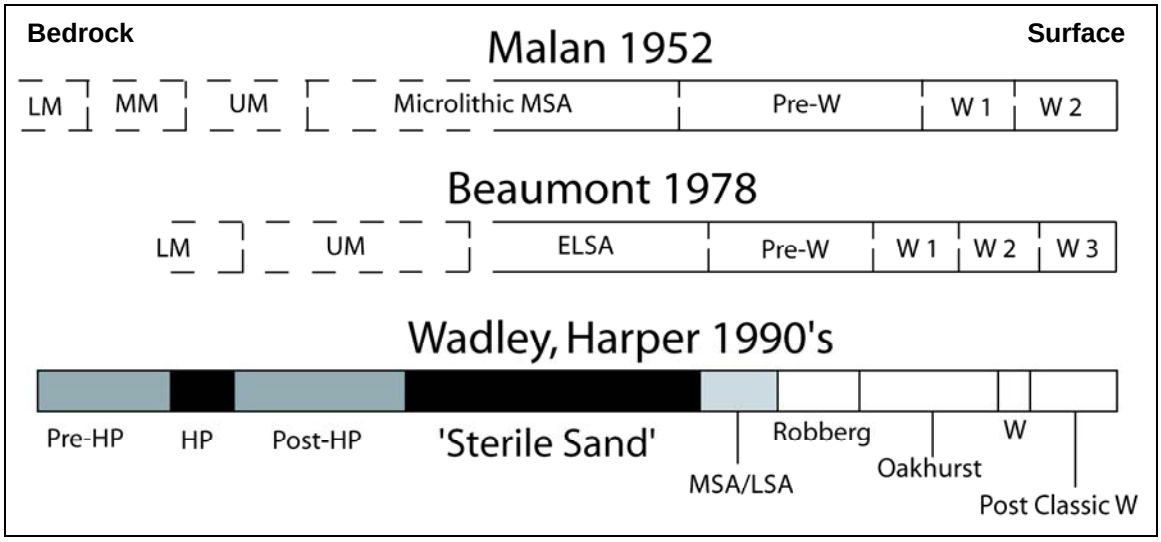

Figure 2. 2 Interpretations of Rose Cottage Cave Lithostratigraphy. LM – Lower Magosian, MM – Middle Magosian, UM – Upper Magosian, HP – Howiesons Poort, W – Wilton. After (Wadley & Harper, 1989; Wadley, 1991; Wadley & Vogel, 1991).

2.2 Palaeo-environmental reconstruction at Rose Cottage Cave

Human adaptive strategies recorded in archaeological sites must in some way accommodate climatic and ecological changes. Currently the best evidence for environmental change during the Quaternary is provided by data recovered from Antarctic ice cores such as the Vostok core (Tyson *et al*., 2001). Other climatic variations are observable through oxygen isotope variations in foraminifera from deep-sea cores (Pillans *et al*., 1998) and define the major warm-cold transitions that characterised the movements of ice sheets derived from the Milankovitch Astronomical Theory (Milankovitch, 1941).

The majority of the environmental evidence from RCC dates between 23 000 years ago and the present. Charcoal and faunal assemblages from RCC (Engela, 1995; Esterhuysen, 1996) provide a basis for our contemporary understanding of palaeo-environmental change in the Caledon river valley (Mitchell *et al.,* 1998). The charcoal analysis shows two vegetation regimes: heathland vegetation during the Pleistocene suggesting cooler dry conditions

and woodland vegetation typical of the Holocene (Wadley *et al.,* 1992). This is complemented by an environmental archaeomagnetic proxy record that suggests an oscillating cooler climate for the late Pleistocene levels with the lowest temperatures occurring during the Last Glacial Maximum (LGM) (Herries & Latham, 2002). The Holocene presents woodland species probably found on the hillsides, and grassland similar to today (Wadley, 1997). Micromammal samples taken from levels dating from 8 500 years ago until 500 years ago indicate an early Holocene wet phase, a climatic optimum in the mid Holocene, and oscillating events in the late Holocene including the Little Ice Age (Avery, 1997).

Pollen spectra from the sites of Elim, Graigrossie and Cornelia near the town of Clarens, approximately 100 km north-east of RCC, suggest a cooler wetter climate between 23 000 and 20 000 years ago (Scott, 1989, Scott *et al.,* 1995, 1997). Studies at both RCC and Tloutle shelter in Lesotho have yielded a proxy climatic history from 13 500 years ago to 5 000 years ago for the Caledon river valley (Esterhuysen & Smith, 2003). Although the period is regarded as a warming interval, data from these two sites suggests a series of oscillating warming and cooling events (Esterhuysen & Smith, 2003).

The opportunity now exists to extend the understanding of palaeo-environments and climates in the Caledon river valley past the limit of the radiocarbon dating technique. With the developments in OSL dating correlation between archaeological and environmental chronologies can be achieved by cross-checking absolute dates against oxygen isotope stages. A basic outline of the oxygen isotope stages is presented in figure 2.3. The last glacial/interglacial cycle according to variations in foraminifera reveals that a regional manifestation of global warming occurred around 125 000 years ago in the western Indian ocean (Tyson & Partridge, 2000) known as Oxygen Isotope Stage (OIS) 5e. A general trend of cooling occurred thereafter, reaching full maturity about 18 000 years ago in the Last Glacial Maximum (LGM) (Pillans *et al*., 1998). Complementary evidence for post glacial warming in southern Africa after the LGM comes from local speleothem data (Holmgren *et al.,* 2003) confirmed for RCC by proxy pollen records from the

surrounding area (Van Zinderen Bakker, 1976; Wadley *et al.,* 1992) and charcoal / faunal analysis from the site itself.

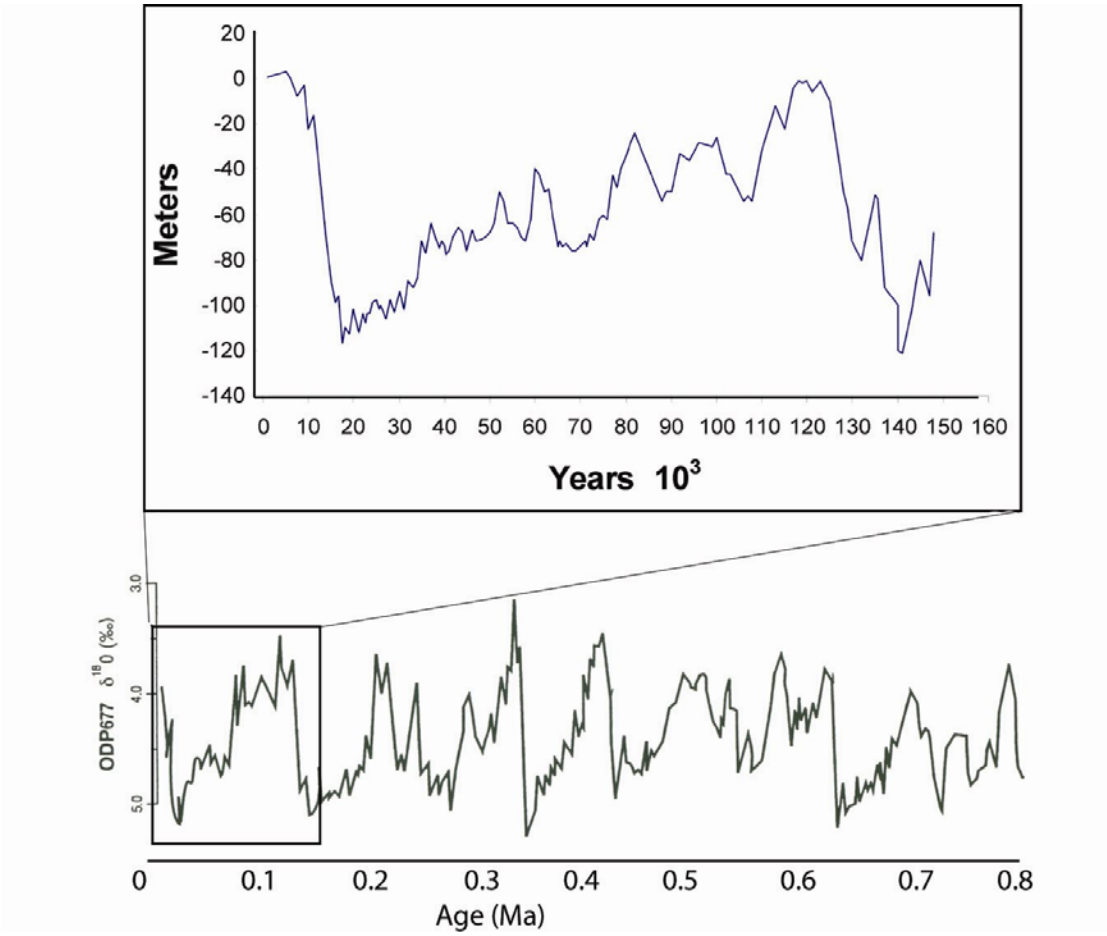

Figure 2.3 (top) Sea level changes for the last 150 ka derived from core V19-30 isotope record, Huon Peninsula. (Bottom) isotope record of ODP Site 677 (modified from Pillans *et al.,* 1998).

2.3 The archaeology of Rose Cottage Cave

The currently accepted Stone Age sequence for RCC is that derived by P.N. Harper and L. Wadley, who excavated through the remaining sections of Malan's excavation to bedrock, a depth of over 6.5 metres. The MSA lithic classification used at RCC by Wadley and Harper is after Singer & Wymer (1982). The sequence, taken from squares If, Ig, Hf, Hg and Hf (see Figure 2.1) begins with a pre-Howiesons Poort MSA II stone tool assemblage (layers LEN, KUA and KUB) consisting of a few points, knives and some scrapers.

They are however, near sterile in artefact accumulation (Harper, 1997). The overlying 15 levels (EMD to SUZ) present backed tools characteristic of the Howiesons Poort (Wadley, 1997) and are representative of a relatively continuous and intense occupation at the cave. Harper (1997) interprets the replacement of formal MSA tools in the pre-HP layers as technological discontinuity, and according to him technological continuity is only regained in the post-HP levels.

The post-Howiesons Poort or MSA III (levels ANN to THO) show a decline in the production of flake blades and an increase in end flake production (Wadley, 1997). Above the post-HP are the 'almost sterile' orange sands (levels MAD to KAR), that span over a metre of deposit (Harper, 1997). Samples taken by K.W. Butzer in 1977 indicate a ^{14}C date of 23 000 B.C. for the top of the sterile layers. Beaumont and Mason submitted samples all dating to > 40 000 years ago and Wadley obtained two dates for the 'orange sands' of 34 375 B.C. and 36 609 B.C. (see Appendix A). The ^{14}C data then suggests a period from 23 000 to > 40 000 years ago for the sterile sands (Wadley & Vogel, 1991). Figure 2.4 presents the stratigraphic horizons of the MSA sequence and shows the positions from where OSL samples were taken.

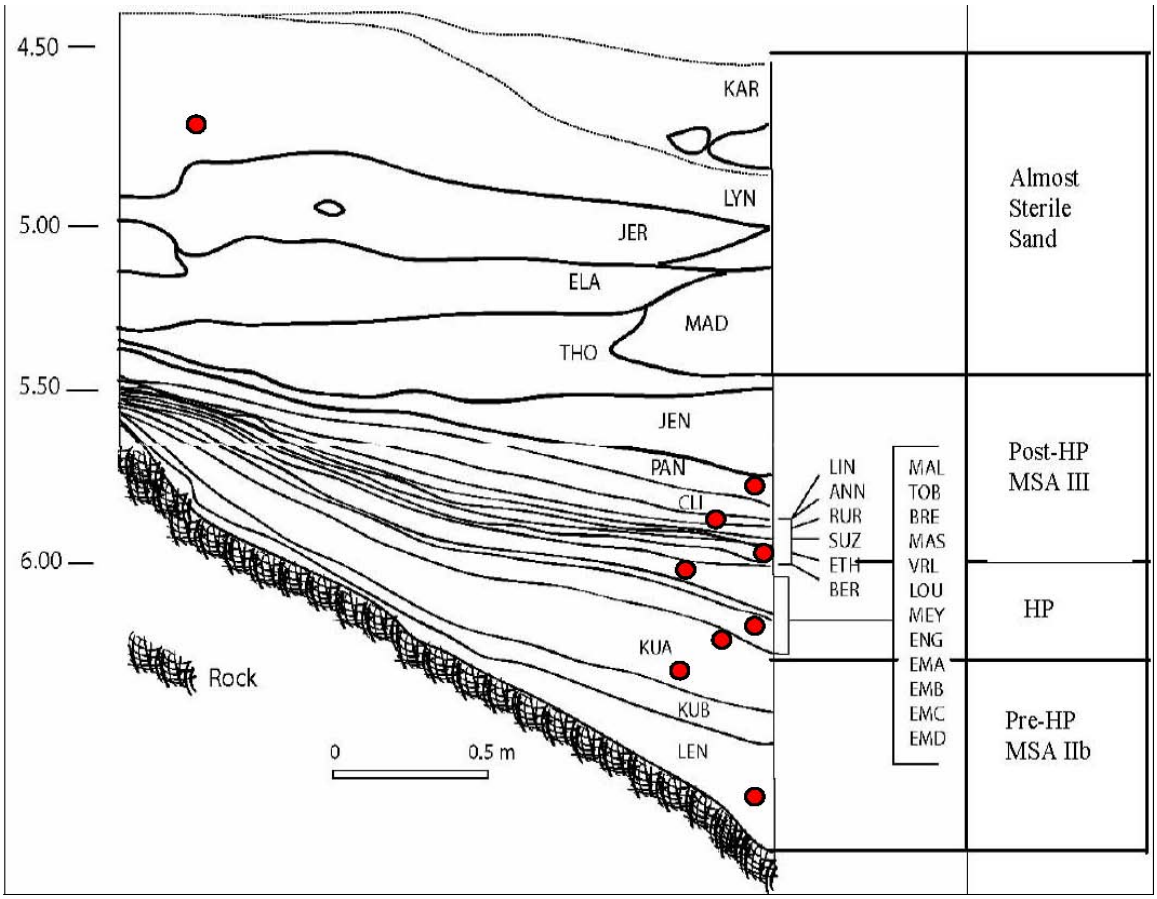

Figure 2. 3 Cross section of MSA levels from the Harper excavation, squares If, Ig and Ih, modified from Harper, 1997. Note the finely stratified Howiesons Poort layers.

The layers directly above the 'sterile sands', up until and including layer Ru, are recognised as the final MSA phase. Layers G2 and G represent a MSA/LSA transition (Clark, 1999, 1997a, 1997b; Wadley, 1997) and contain more than 65 000 stone artefacts, representing one of the largest assemblages of this type in southern Africa. This assemblage is similar to a transitional assemblage at Sehonghong shelter (Clark, 1997a; 1997b) and radiocarbon dates to 21 735 B.C. with a one sigma range (21 921 – 21 549 B.C.) (see Pta 5598 Appendix A).

The LSA layers at RCC are well-stratified into the Robberg, Oakhurst, Wilton and post-classic Wilton industries (Clark, 1997a; Wadley, 1991; 1997). These layers have a chronological radiocarbon sequence (see Appendix A) and form the basis for testing the OSL protocols. Wadley (1991) excavated a 32m^2 area in the western portion of the cave. Levels Db, Lb and DCM contain the first

clear evidence for a Robberg industry (Clark, 1997b). The industry was first officially recognised in Nelson Bay Cave on the Robberg Peninsula (Klein, 1974). It was however, first observed in South Africa at RCC by Abbé Henri Breuil in the 1950s (Wadley, 1996). The age of the Robberg Industry in South Africa is between 22 000 and 12 000 years ago (Deacon & Deacon, 1999), ending just before the Pleistocene/Holocene transition. The Robberg at RCC however, is thought to end roughly 10 000 years ago (Wadley, 1991).

The majority of the formal stone tool assemblage of the Robberg Industry consists of thin parallel-sided bladelets (Wadley, 1997). Binneman (1997) suggests that the bladelets at RCC were produced by bipolar flaking and usewear traces along the lateral surface indicate that they were used predominantly for cutting or sawing. The majority of the molecular residues found on these tools suggest they were used for delicate work on plant material rather than meat (Williamson, 1997). The Industry also contains the earliest bone points found at RCC, as well as very few ostrich eggshell fragments (Wadley, 1996). Wadley (2000) suggests a more structured use of space in the Robberg levels as compared to the MSA/LSA transition. A variety of hearths create an arc around the entrance boulder where they are protected from natural weather processes (Wadley, 1996).

Above the Robberg industry is the Oakhurst (levels Ja, Ph, Cm, H and O) (see Figure 2.5) characterized by a variety of scrapers and microlithic side struck flakes (Wadley, 1991). At other sites in South Africa the Oakhurst commences about 12 000 years ago and ends about 8 000 years ago. With the late transition from the Robberg at RCC, the Oakhurst begins roughly 10 000 years ago and ends 2 000 years later (see Appendix A). There is a marked increase in trade material in the Oakhurst (Wadley, 1991). This is overlain by the ‘Classic Wilton’ (level Pt) and ‘post-Classic Wilton’ (levels Mn, A2 and A). The post-Classic Wilton contains assemblages with pottery and ostrich eggshells, and has a high frequency of retouched tools (Wadley, 1997). The presence of a cowrie shell and interpretations of the rock art indicate contact with coastal peoples. Thorp’s (1997, 2000) analysis of the pottery from layers Mn and A suggests interaction with Sotho-speaking

groups. Figure 2.5 presents the stratigraphic horizons of the LSA sequence taken from the Wadley excavation. The dots indicate the positions from where luminescence samples were taken and cover the entire LSA lithostratigraphic sequence.

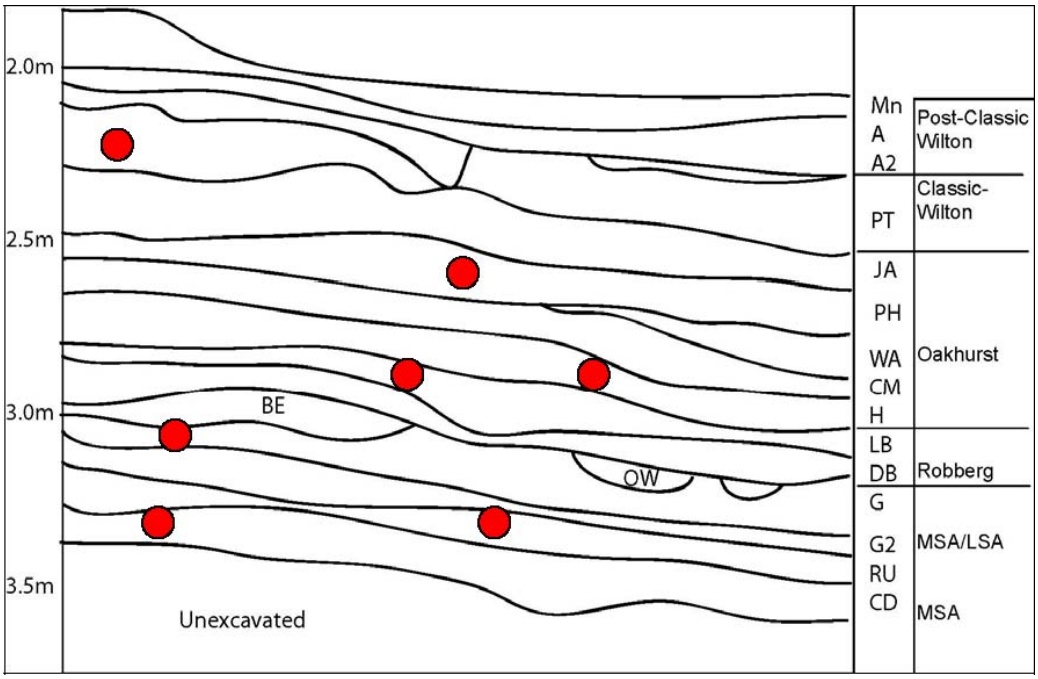

Figure 2. 4 LSA stratigraphy of Rose Cottage Cave, north section, squares O5 and N5, modified from Clark (1997b).

2.4 Sampling strategy of Rose Cottage Cave sediments

A total of 16 OSL samples were taken from the base of the excavation up to the top of the excavation, but due to time constraints and machine availability only 14 were dated. 11 samples were taken from the MSA section up to the base of the 'sterile sands' and cover the main archeological periods. Five samples were taken from the LSA layers. These samples were taken from layers associated with radiocarbon dates so that correlation between dating methods could be checked. Three prior luminescence dating studies have been conducted at the site focusing on the MSA deposits with the main aim of establishing an age for the HP. These include TL dating of sediments (Woodborne & Vogel, 1997; *pers. comm.*), TL dating of burnt lithics by H.

Tribolo and H. Valladas (Tribolo, 2003), and OSL dating of sedimentary deposits by A. S. Murray (*pers. comm.*). These studies place the upper levels of the 'sterile sands' at 33 000 years ago, the post-HP between 44 000 and 60 000 years ago, the HP to between 60 000 and 70 000 years ago and, the pre-HP as >70 000 years ago. Table 2.1 presents a schematic outline of where the luminescence samples were taken from

Table 2. 1 Sampling strategy for Rose Cottage Cave samples

RCC OSL samples			
Depth (m)	**Layer**	**Sample**	**Lithostratigraphy**
	MN **A** **A2**		***Post-Classic Wilton***
	PT	RCC 17	**Classic Wilton**
2.5	**JA** **PH** **CM** **H**	RCC 22 RCC 21	**Oakhurst**
	LB **DB** **BE**	RCC 20 RCC 10	**Robberg**
	G **G2**	RCC 19	**MSA/LSA Transition**
3	**RU** **CD**	RCC 9 RCC 18	**MSA IV**
4.8	**LYN**	RCC 16	**Almost "sterile" sand**
6.8	**CLI** **ANN**	RCC 6	**Post-HP MSA III**
6.9	**ETH** **BER** **EMC**	RCC 14 RCC 7 RCC 13	**HP**
6.5	**KUA** **KUA** **LEN**	RCC 12 RCC 8 RCC 11	**Pre-HP MSA IIb**

Sampling must be carried out in a manner that prevents the stimulation of trapped electron populations in quartz grains (Murray & Wintle, 2000). During sample collection at Rose Cottage Cave sample tubes (50 mm diameter) were inserted into the stratigraphy under a light-tight tarpaulin using a subdued red light filtered torch.

2.5 Isolation of quartz from Rose Cottage Cave

In the laboratory the sediment samples underwent chemical treatment to remove carbonates and organic matter, and then physical separation to isolate a single mineral fraction (quartz or high potassium feldspars). The process of quartz purification is given in detail by Aitken (1985), Stokes (1992), Huntley *et al*. (1993), and Roberts *et al.* (1994).

In this study the samples were suspended in concentrated hydrochloric acid to remove the carbonates ($CaCO_3$) and Iron (Fe). Organics were removed by adding either NaOH or H_2O_2, then dried and bulk sieved into different size fractions. Magnetic particles were removed using a Franz magnetic separator. The size fraction used in this study was determined by the grain size distribution of the sample and generally corresponded to 106-150 µm and 180-212 µm (see Appendix B). Quartz and potassium feldspars were then separated on the basis of density by suspension in heavy liquids (Mejdahl, 1985). A sodium polytungstate solution of specific gravity 2.62 was used for the isolation of quartz (Stokes, 1992; Huntley *et al.,* 1993; Roberts *et al.,* 1994). The samples were then etched in 40% hydrofluoric acid (HF) to remove any contribution from alpha radiation and any remaining plagioclase feldspars.

3 OSL DOSE DETERMINATION: THEORY AND EQUIPMENT

3.1 OSL Theory

The production of OSL dates using quartz is based on three criteria:

- A flux of energy from natural radioactivity
- A reproducible luminescence response to radiation by the mineral (a natural dosimeter)
- A zeroing event.

Minerals that make up sedimentary deposits, such as quartz and feldspar grains act as natural dosimeters. They absorb and store energy from the decay of natural radioactivity found in the surrounding environment. This energy is produced by trace amounts of uranium (U), thorium (Th) and potassium (K) found in the surrounding soil matrix. The decays relevant to luminescence dating consist of alpha (α), beta (β), gamma (γ) and cosmic radiations. Energy from these decays force valence electrons inside the quartz crystals to diffuse to higher energy “traps”. The process whereby stored electrons are released is called zeroing or “bleaching” and occurs naturally during sediment mobilisation (exposure to sunlight), or through heat, that could be related to archaeological phenomena such as hearths. The basis of this process is simplified in Aitken’s (1985) schematic of the transfer, storage and release of energy in a quartz grain (figure 3.1).

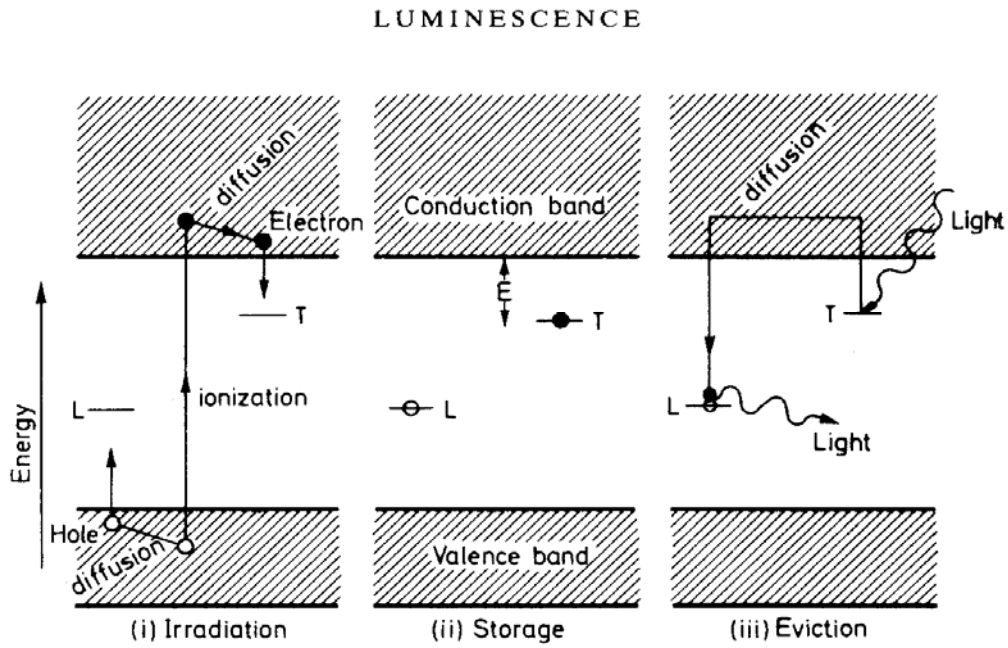

Figure 3. 1 Radiation energy causes valence electrons to be transferred to the conduction band. In this process positively charged 'holes' are formed in the valence band. The holes assume a high energy state because of their electron deficiency. After diffusion the electrons either recombine with holes or get trapped at defects or impurities within the mineral lattice. These traps occur at different energy levels and have different thermal stability. When trapped electrons are stimulated by either light or heat they diffuse in the conduction band and recombine with the holes. The resulting energy emission can be in the form of heat or light. Holes that produce light during electron recombination are known as luminescence centres (Aitken, 1998:44).

Figure 3.1 can be used to explain that radiation energy from the surrounding environment is transferred to the valence electrons in a quartz grain. These electrons diffuse to a high energy state called the "conduction band" (Bøtter-Jensen, 1997). The movement of an electron out of the valence band is associated with the formation of a positively charged "hole" that has a higher energy state than the valence band. Diffusion of high energy electrons in the conduction band causes them either to recombine immediately with the holes, or they become trapped in local energy minima caused by defects or impurities in the crystal lattice. The mechanism of electron trapping in quartz grains is dependent on the radiation dose rate that derives from the surrounding matrix. If this is constant, then the accumulation of trapped electrons will be a time dependent function. An energy input in the form of

heat or light transfers sufficient energy to the trapped electrons for them to escape the trap. These electrons either recombine with trapped holes called luminescence centres and release energy in the form of light or recombine with 'hole' traps that do not result in photon emission; these are called non-radioactive centres. The accumulative light that is released is called luminescence and is a direct measure of the de-trapped electron population.

There are many different electron trap types relating to different impurities within a crystal lattice. These traps have varying energy levels that have different thermal stabilities and optical depletion rates. Three easily identifiable trap populations in quartz correspond to thermal treatment at 110°C, 325°C and 375°C (Spooner *et al.,* 1988) respectively. Wintle & Murray (1998) have shown that the major proportion of a luminescence signal is produced by the charge responsible for the 325°C TL peak. These energy traps exhibit different bleaching behaviour: the 375°C peak bleaches more slowly than the 325°C peak and is referred to as the slow bleaching peak (SBP). The 325°C peak is a faster bleaching peak (FBP) and has been used extensively in dating (Huntley *et al.,* 1993). It has been demonstrated (Murray & Wintle, 1999a) that samples dominated by a fast bleaching component from the 325° TL peak (lifetime of 10^8 years at 20°C) can produce ages with little complications. Optically stimulated luminescence obtained from quartz using light stimulation between 420 and 520 nm yields a peak luminescence emission at 340 nm. This is comparable to the emission of the 110°C and 325 ºC TL traps in the ultra-violet region and the 375 ºC TL trap in the blue region (Bøtter-Jensen & Duller, 1992). Infra-red stimulation using a wavelength at around 880 nm does not significantly affect quartz (Stokes, 1992; Duller, 2003) although it does stimulate a luminescence signal in feldspars; the signal that is produced is called infra-red stimulated luminescence (IRSL).

3.2 Calculation of the depositional age of sediments

The depositional age of sediments is calculated as the time since electron traps were previously emptied or bleached until the present. The rate at which these traps are repopulated is determined by the environmental dose rate expressed in Gy/ka (radiation dose received per unit time). Several methods can be employed to evaluate the dose-rate. In this study the radionuclide concentration (ppm) of Th and U were determined in the laboratory by Thick Source Alpha Counting (TSAC), and ^{40}K was determined by XRF, then converted into Gy/ka. In the field, in situ gamma measurements were performed with the aid of a portable field gamma spectrometer (FGS). The dose rate can then be compared with the accumulated dose (D_e) of the sample to calculate the age using the *age equation*:

$$Age\,(ka) = \frac{Equivalent\ laboratory\ dose\,(D_e)\,(Gy)}{Dose\ rate\,(Gy/ka)} \qquad \textbf{Equation 3. 1}$$

3.3 Determination of trapped electron populations in the laboratory

The measurement of the trapped electron population in the laboratory is accomplished by a similar mechanism to the zeroing event. The quartz is stimulated (with heat or light) with sufficient energy to de-trap the electrons. In OSL dating of quartz, isolated grains are stimulated using continuous wave OSL (CW-OSL), using blue LEDs for 40 seconds at 90% power i.e the wavelength and illumination intensity are fixed. The signal created by the recombination of electrons with luminescence centres results in an OSL decay curve (figure 3.2).

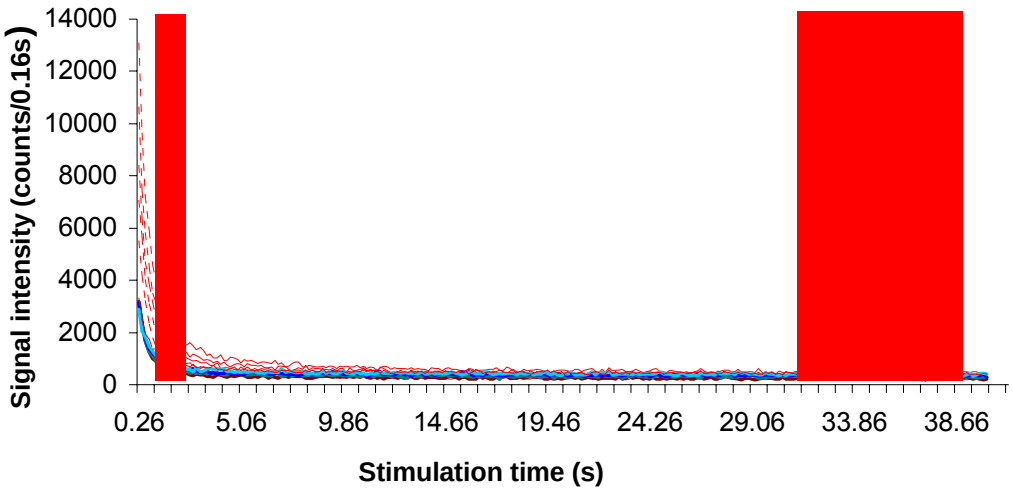

Figure 3. 2 Representation of eight decays from the same sample using different preheat temperatures. The two red bars indicate the area of integration for the signal and background. The blue line represents stimulation carried out after a 300ºC preheat indicating partial depletion of the 325ºC trap.

The resulting luminescence signal observable in these OSL decay curves is a direct measure of the trapped electron population and is proportional to the charge trapped since the last depositional event. This measurement can be used to establish the radiation dose (*Equivalent Dose*, D_e) the sample received since burial, by reproducing the amount of radiation that is required in the laboratory to match the natural OSL signal. The D_e is then determined by comparing the natural OSL signal with an OSL signal produced from a range of artificial irradiations administered in the laboratory. In this study samples were irradiated using a calibrated ^{90}Sr beta source positioned 5mm from the sample when in the irradiation position (Bøtter-Jensen *et al.,* 2000) and delivering a dose rate of more than 10 Gy/min (0.18 Gy/sec).

The reconstructed growth of the luminescence signal in relation to the applied dose is called the *dose response curve* or the *growth curve*. Artificially created decay curves are converted into dose response curves that are used to project the natural OSL measurement onto a radiation axis. Figure 3.3 below shows a representation of a dose-response curve that can be used to asses the D_e of a sample.

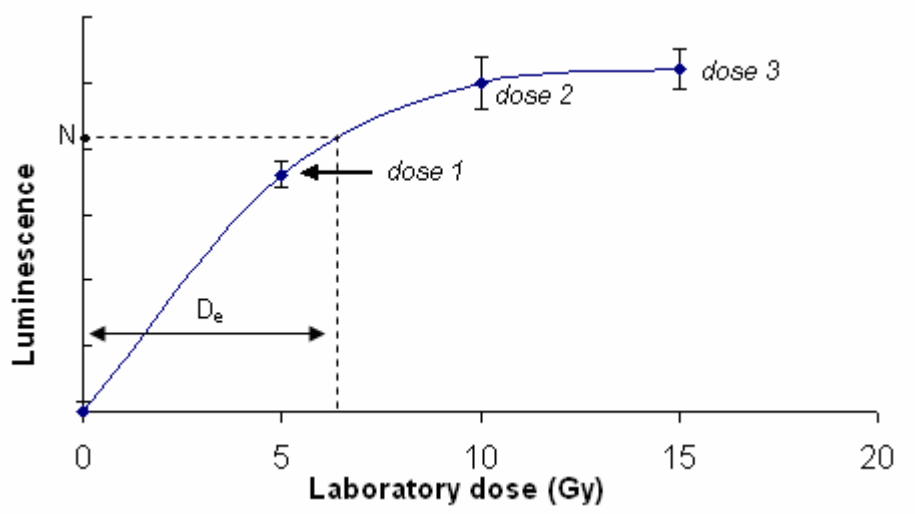

Figure 3. 3 Regenerative growth curve. Each data point has been given a laboratory dose after the aliquot was bleached. The D_e is determined as the intercept between the natural measurement (N) and the dose response curve (modified from Aitken, 1998).

3.4 Problems associated with OSL dating

Several problems exist in OSL dating of sediments. These relate to the history of the sedimentary grains (adequate light exposure prior to deposition, contamination) and the physical properties of the quartz grains at a particular site. One problem in particular with archaeological sites is associated with a mixture of grains from adjacent stratigraphic layers or contamination from roof and wall disintegration. Jimnium Rock Shelter in northern Australia is a good example of how contamination can lead to an overestimation of the depositional age of the sediments (Fullagar *et al.,* 1996; Roberts *et al.,* 1998, 1999). At Rose Cottage Cave sediments were assumed to have been deposited by a mixing of water lain sediments, wind blown sediments and eroded cave roof and wall material (Butzer, 1984a, 1984b).

For these sediments analytical approaches used to determine the bleaching history of the grains (Bailey, 2003a, 2003b; Bailey *et al.,* 2003) were a critical requirement of the dating process. An assumption is that the quartz OSL signal consists of components defined in terms of the speed at which they bleach (Bailey *et al.,* 1997, Jain *et al.,* 2003). In most quartz grains there are a

minimum of three OSL components (Bailey *et al.,* 1997), namely the slow, medium, and fast components. Jain *et al.* (2003) have identified at least seven OSL components in quartz, referred to as the UltraFast (UF), Fast (F), Medium (M), Slow 1 (S_1), Slow 2 (S_2), Slow 3 (S_3) and Slow 4 (S_4) components. Samples that are dominated by a medium or slow component have a disadvantage in that partial bleaching is more probable.

Two commonly used methods to detect partial bleaching are categorised as distribution methods and signal analyses methods (Bailey, 2003a; 2003b). Distribution methods rely on the interpretation of the spread of D_e values, whereas the signal analysis method compares various components within the decay of individual OSL signals. The use of a signal analysis protocol to identify incomplete signal resetting has been used in this study. The method uses a single aliquot procedure (Duller, 1991) and calculates D_e as a function of time ($D_e(t)$), where time is defined as the stimulation time of the blue diodes in the reader, and gives a time dependent depletion characteristic of the signal. In the $D_e(t)$ method of Bailey (2003a, 2003b) the OSL signal must consist of thermally stable fast bleaching and a slow bleaching components. The assumption is that if all the OSL components were adequately zeroed, then a consistent age would be obtained from all portions of the signal. If the sample is partially bleached then a slower bleaching component (medium component) would yield a greater residual signal i.e. indicate a greater age.

Problems associated with the physical characteristics of quartz are commonly called luminescence sensitivity changes and they manifest as variability in the dose response curve. Changes in OSL sensitivity are related to the characteristics and behavior of OSL traps. Sensitivity changes that occur during D_e determination can be observed as a function of preheating as well as measurement cycle and relate to the distribution of charge among the different kinds of traps. The sensitivity changes found in shallower TL traps are removed by thermal treatment. The use of a preheat range between 160°C and 300°C has been suggested (Murray *et al.,* 1997) in order to isolate a signal derived from thermally stable traps and to equalize sensitivity between the natural and laboratory irradiated measurements.

3.5 OSL Instrumentation

An increasing demand to produce large amounts of measurements has driven the need for automated luminescence systems, and advances in understanding luminescence behaviour (particularly in quartz) has led to improved accuracy and precision through improved laboratory protocols. The development of the conventional SAR protocol (Murray & Wintle, 2000) (discussed in chapter four) and the introduction of single grain dating (Lamothe *et al.,* 1994) has recently led to the development of automated single aliquot/single grain systems. These systems need to fulfil the following requirements:

- A calibrated beta irradiation source
- A heater element with exceptional temperature control
- An optical stimulation system
- A single grain XY attachment unit, and
- A light emission detection unit (photomultiplier).

The Risø automated OSL/TL DA-15 (figure 3.4) unit meets these criteria and was used in this study. It is fitted with a standard photomultiplier (PM) tube, an OSL XY unit for single grain measurements, four optical stimulation systems, a thermal stimulation system, and an internal beta irradiation source. The OSL attachment is built up of 10 clusters of blue LEDs, positioned 20 mm in distance from the sample. The LEDs are arranged in four clusters each containing six LEDs and deliver > 40 mW/cm^2 at the sample position. To minimise scatter a green long-pass GG-420 filter is placed in front of each cluster (Bøtter-Jensen *et al.,* 2003). A second stimulation system comprising 24 IR LEDs (875 nm) are arrange in six clusters in between the blue LEDs. They deliver approximately 135 mW/cm^2 at the sample position. Both IR and blue diode arrays are equipped with optical feedback systems that are used to stabilise their emission power (Bøtter-Jensen *et al.,* 2003).

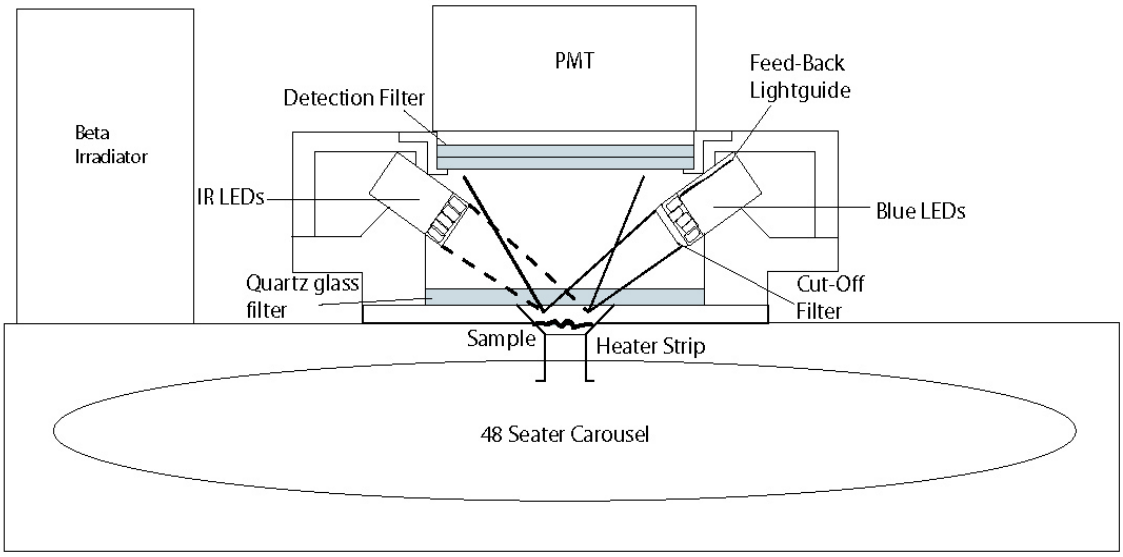

Figure 3. 4 Schematic of the Risø TL/OSL DA-15 reader with new IR/Blue LED OSL unit attachment (after Bøtter-Jensen *et al.,* 2003).

The XY single grain attachment (see figure 3.5) comprises of a 150 mW IR (830 nm) laser and a 10 mW (532 nm) green laser (Bøtter-Jensen *et al.,* 2003). This enables the user to perform routine measurements on single grains of quartz or feldspar. The grains are arranged in an aluminium disc, consisting of a 10 x 10 hole matrix, each hole being approximately 300 µm wide and 300 µm deep. The laser focuses on a 50 µm spot on each grain as required when performing measurements.

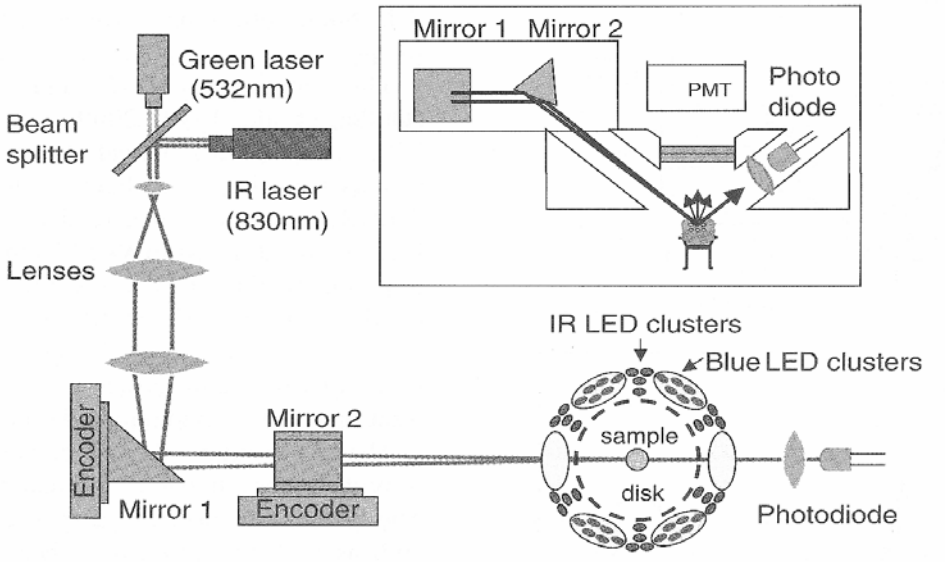

Figure 3. 5 Schematic of single-grain OSL attachment (from Bøtter-Jensen *et al.,* 2003).

The beta irradiation attachment on the Risø TL/OSL DA-15 reader is positioned 5mm above a sample in the irradiation position (Bøtter-Jensen *et al.,* 2000) and is fitted with a ^{90}Sr source with activity 1.48 GBq (40 mCi). This source is a 0.5 MeV beta emitter with a half-life of 28.5 years. Its daughter is ^{90}Y, a 3 MeV beta emitter with a half-life of 64.1 hours and a 230 keV/480 keV gamma emitter with a half life of three hours. The final product is stable Zirconium 90 (^{90}Zr). Although the typical strength of such a source is ~ 5 Gy/min (0.1 Gy/sec) at the sample irradiation position (Bøtter-Jensen *et al.,* 2000), the QUADRU ^{90}Sr source delivers a dose rate of more than 10 Gy/min (0.18 Gy/sec). A consequence of such a strong irradiation source is the effect of 'cross-talk' to neighbouring discs on the carousel. The cross-talk is defined as the radiation dose to samples in the vicinity of the intended sample. The extent of cross-talk or 'cross-irradiation' to adjacent samples can be as high as 0.1735 ± 0.0004 % (Bøtter-Jensen *et al.,* 2000). However, Bray *et al.* (2002) have reported 0.0055 ± 0.012% less than Bøtter-Jensen *et al.* (2000) by 2 orders of magnitude.

The beta source was calibrated by using gamma-irradiated (5 Gy) calibration quartz (180-212 µm) provided by A.S. Murray. A total of 35 aliquots were measured using a standard SAR protocol (Murray & Wintle, 2000). The results are presented in figure 3.6 in the form of a radial plot and a probability density plot displaying how a D_e of 5 Gy relates to the ^{90}Sr source in terms of s, where s is defined as the stimulation time of the beta source in the reader, in seconds irradiation.

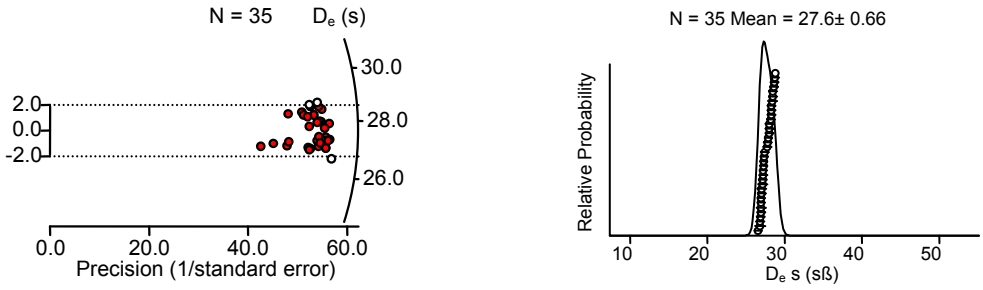

Figure 3. 6 Results of calibration quartz having a gamma dose of 5 Gy. Measurments were performed on 180-212 µm quartz fractions using a 5mm mask size.

The heater strip in the Risø TL/OSL DA-15 reader is made of high resistance alloys. Temperature feedback is achieved using a thermocouple welded to the heater strip (Bøtter-Jensen, 1997), and rapid cooling is done with the use of nitrogen that flushes the measurement chamber. To test the accuracy of the heater plate and stability of preheating, a measurement protocol was carried out using a 180-212 µm fraction of bleached calibration quartz. The results presented in figure 3.7 were performed on one aliquot, 6 mm in diameter, that was given a dose of 9 Gy and a test dose of 1.8 Gy, repeated for ten measurement cycles. Stimulation was carried out at 125 °C. The sensitivity corrected luminescence signal (L_x) divided by the test signal (T_x) shows the effects of charge transfer from the 110 °C trap and depletion of the 325 °C trap at higher preheat temperatures. This is similar to sensitivity changes observed by Aitken & Smith (1988) when preheating between 220 °C and 300 °C. The results display thermal stability between 160 °C and 260 °C, causing the least amount of thermal erosion to the 325 °C OSL trap and providing a good indication that the heater plate is working adequately.

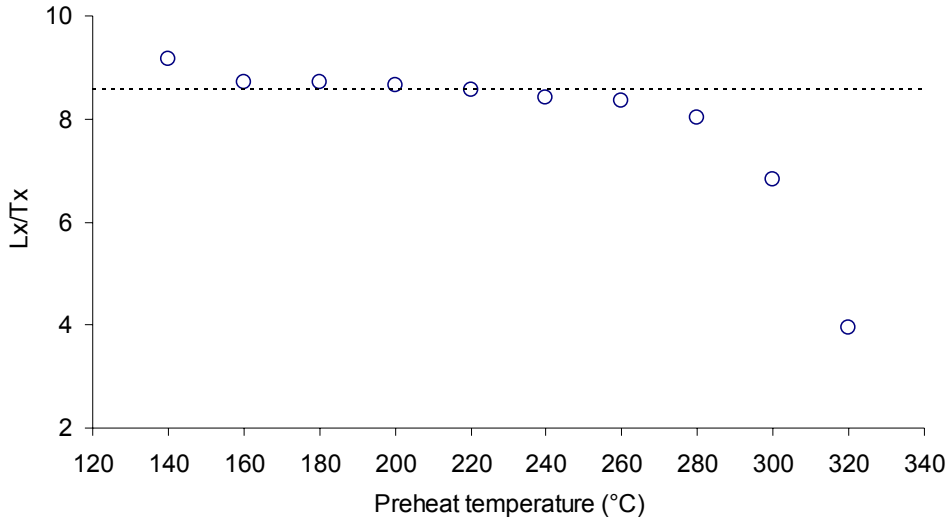

Figure 3. 7 Heater plate test, showing charge transfer before 160 °C and after 260 °C on a typical quartz sample.

A systematic error was calculated for the Risø TL/OSL DA-15 reader by repeatedly irradiating, preheating and stimulating the same aliquot ten times. Preheating was carried out at 260°C and OSL stimulation was measured at

125°C. A linear trend was fitted through the data points. The scatter above and below the line represented the standard deviation of the data from the trend line. The relative standard error arising from instrumental uncertainty is therefore the error arising from variability around the fitted line minus the error that arises from counting statistics and was calculated as 1.8% and was subsequently used for all calculations in this study.

3.6 D_e Determination

3.6.1 Additive and Regenerative dose protocols

The protocols for measuring the equivalent dose (D_e) comprise two approaches: the additive dose and regenerative dose methods (Aitken, 1998). Both approaches begin with the determination of the natural luminescence signal, and then simulate the growth of the luminescence signal using a calibrated laboratory radiation source. In the regenerative approach, however, samples are first bleached to near zero before each dose is administered to stimulate the shape of the luminescence growth curve.

In both methods measurements are carried out on aliquots of pre-treated mineral extracts mounted on silicate that is sprayed onto the discs (steel or aluminium) through a predetermined mask size. This limits the area of oil application, and hence the number of grains that will adhere to the disc. Both additive and regenerative approaches have employed multiple and single aliquot protocols in order to obtain accurate estimates of D_e. The determination of D_e is then the use of laboratory protocols that can be employed to establish the equivalent laboratory dose the sample received since deposition until the present. In the single aliquot approach first developed by Duller (1991) for feldspar dating, all measurements are carried out on the same aliquot (Aitken, 1998). This has an advantage over multiple aliquots by avoiding the need to normalise inter-aliquot variability. The single aliquot regenerative dose (SAR) protocol (Murray & Roberts, 1998; Murray & Wintle, 2000) was used in this study as a means to determine D_e values.

The main concern in D_e determination is related to OSL sensitivity changes between natural and laboratory induced irradiations (Wintle & Murray, 1998; Murray & Wintle, 1999b). Sensitivity changes are attributed to the change in luminescence efficiency (OSL per evicted electron) (Aitken, 1998) and the rate of trap filling per unit irradiation (Murray & Wintle, 2000). It has been shown that sensitivity changes are proportional to the intensity of the 110°C TL peak (Aitken & Smith, 1988) in quartz. Zimmerman (1971) created a model for sensitisation of the 110°C TL peak and demonstrated how high temperature annealing can activate sensitivity changes. Most of this type of charge transfer observable in shallow energy traps (Murray & Wintle, 1999) can be removed through preheating. Precaution must be taken, however, due to an increase in recuperation or "charge transfer" at higher preheat temperatures by thermally stimulating higher energy traps (Aitken & Smith, 1988).

3.7 The SAR Protocol

During each measurement cycle in the SAR protocol three thermal treatments are applied, namely: Preheating, heating during stimulation and a cutheat before each test dose. Preheating is used to redistribute charge in order to compare the natural and irradiated signals. This type of transfer is known as thermal transfer or recuperation and reflects the presence of unstable (slowly bleaching) traps or centres (Wintle & Murray, 1999). Murray & Wintle (2000) recommend that stimulation be carried out at 125°C with a heating rate of 5°C/s to eliminate the influence of charge transfer from the 110°C peak. The cutheat is administered at a low enough temperature as to avoid sensitivity changes in deeper traps and at the same time eliminates unstable charge from the 110°C trap. If an Ultra-Fast luminescence component is detected, Murray & Wintle (2003) have suggested a higher cutheat temperature (e.g. 200° C) to remove this component. The effects of recuperation, monitored with the use of a zero dose measurement (Murray & Olley, 2002), may also be removed with high temperature stimulation such as 240° C for 100s (Jacobs, 2004).

The major advancement brought about by the SAR protocol is the incorporation of a test dose used to correct for sensitivity changes during measurement cycles. Sensitivity corrected dose response curves are created by administering a small test, roughly (10%) of the natural D_e (T_x), is used to monitor sensitivity changes (although the test dose can be any size), followed by a regenerative dose (L_x). Normalisation of this response provides a reasonable correction for sensitivity changes. A generalised measurement sequence, illustrated in figure 3.8 is as follows:

- Aliquots of the sample are divided into eight groups of three and given a dose (D_i) followed by a range of preheat temperatures between 160º and 300º, for ~ 10 seconds. In the first measurement cycle the applied dose is zero and this measurement yields the natural luminescence signal.
- After preheating, the OSL signal (L_x) is measured at 125°C (Murray & Olley, 2002). Note that during the first OSL measurement or natural, no dose (D_i) is given.
- A test dose, in the order of 10% of the natural is administered after each L_x measurement to correct for sensitivity changes. The test dose (D_t) is heated to 160°C to removed unwanted components of the 110°C TL trap (cut heat) and the OSL signal (T_x) is measured at 125°C.
- The cycle is repeated using several different doses for each cycle.

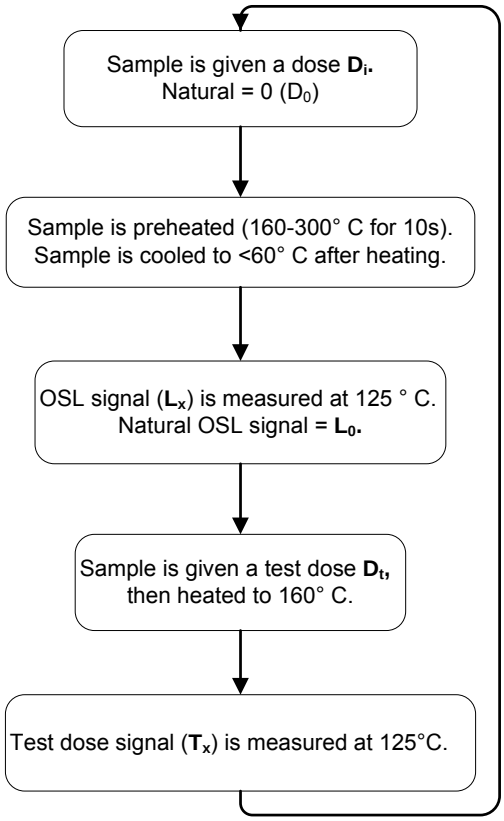

Figure 3.8 Generalised SAR measurement sequence modified from Murray & Wintle (2000)

A sensitivity corrected dose response curve shown in figure 3.9 compares the regenerative dose (L_x) and test dose (T_x) and can be explained by

$$L_{x\,cont.} = \frac{L_x - L_{xbg}}{T_x - T_{xbg}} \qquad \textbf{Equation 3.1}$$

Where:

L_x is the OSL from the regenerated SAR cycle (typically the first 0.2-0.8s of stimulation),

L_{xbg} is the background (slowly depleting portion of the OSL signal).

T_x and T_{xbg} are the test dose signal and background (Stokes *et al.,* 2000).

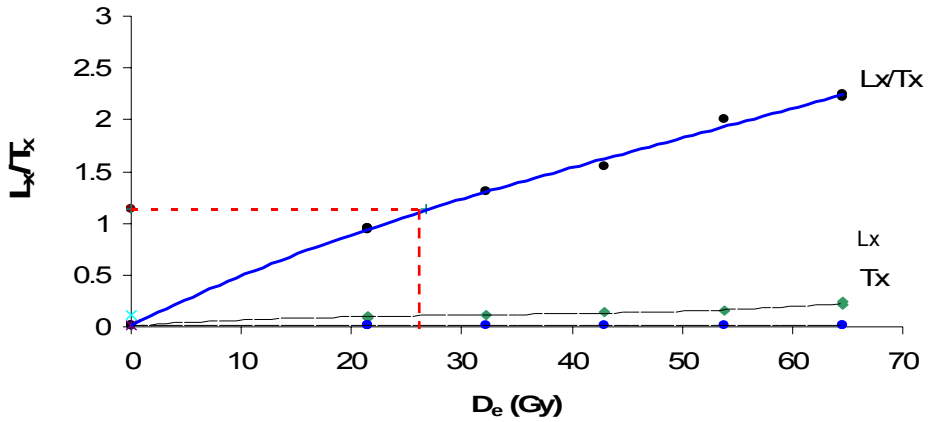

Figure 3.9 A typical SAR growth curve (Lx/Tx), having a D_e intercept of 26 Gy. Note the OSL measurement (Lx) and the test dose (Tx) have been normalised to zero. The ratio between these two measurements is used to construct the corrected (Lx/Tx) dose response curve.

From Figure 3.9 we assume that the signal from the test dose ($\mathbf{T_x}$) uses the same electron traps responsible for the main OSL signal ($\mathbf{L_x}$), therefore giving a good indication of sensitivity change. The test dose uses the OSL of the 110°C TL peak to monitor sensitivity changes associated with temperature and time that occur after irradiation (Murray & Roberts, 1998; Wintle & Murray, 1999; Murray & Wintle, 2000). As noted earlier the use of a preheat range between 160°C and 300°C has been suggested (Murray *et al.,* 1997) in order to isolate a signal derived from thermally stable traps.

Murray & Mejdahl (1999) demonstrated that the relationship between the OSL test dose and the OSL regenerative dose must be linear for sensitivity to be adequately corrected. This linear relationship is demonstrated for quartz (Murray & Mejdahl, 1999; Murray & Roberts, 1998; Murray & Wintle, 2000) by the relationship between the test doses (T_x) and the regenerative doses (L_x). Figure 3.10a below is an example of values of L_x are plotted against T_x for a series of preheat measurements and shows the relationship between two regenerative dose points. In figure 3.10b sensitivity changes that occur in the 110°C TL trap for the same set of data is represented. The regenerative test dose values (T_x) are normalized to T_n (the test dose administered after measurement of the natural) and show the sensitisation process that occurs

during a typical SAR process. There is an initial decrease in sensitivity for the lower preheat temperatures (160°C - 240°C) and an initial increase in sensitivity for the higher preheat temperature (260°C - 300°C).

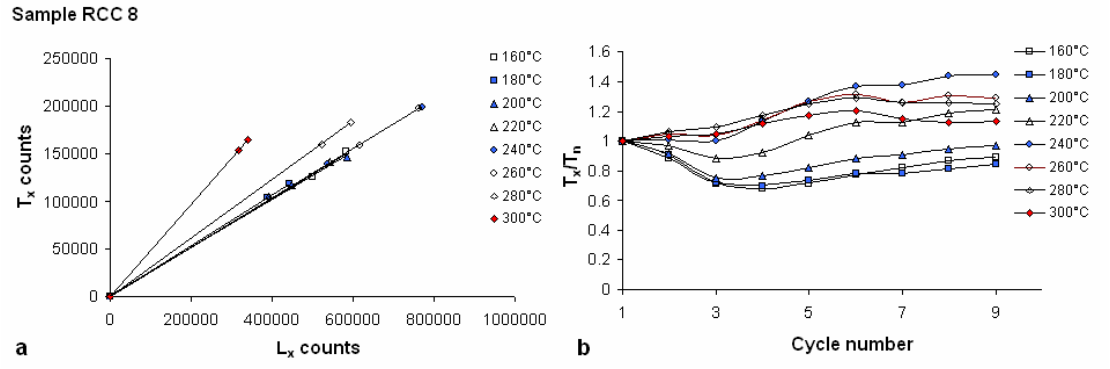

Figure 3.10 Sensitivy changes monitored by the relationship between L_x/T_x and T_x/T_n vs. SAR cycle number. The checks are performed on aliquots using large mask sizes (5mm). The repeated dose points representing L_X/T_x values were obtained through recycling low dose data points. Each paired value is taken as averages from eight different preheat temperatures. The 300°C values in figure 4.2a deviate from the main trend due to thermal depletion of the L_x measurement. For all the temperatures L_x vs. T_x values present a linear relationship. In figure 3.10b the values of T_x are normalized to $T_{n,}$ the lower preheat temperatures show a decrease in sensitivity for the first few measurement cycles. The higher preheat temperatures have an increase in sensitivity for the first few measurement cycles.

3.7.1 Advantages of the SAR protocol

Murray & Wintle (1999a, 2000) demonstrated that a quartz dose response curve is not greatly affected by choice of preheat, provided that sensitivity changes are corrected. Two tests have been suggested (Murray & Roberts 1998, Wintle & Murray, 1999; Murray & Wintle, 2000; Wallinga *et al.,* 2001) to check the reproducibility (Murray & Wintle, 2000) of sensitivity corrected dose curves. The first and probably the most important check is termed the *dose recovery test* (Wallinga *et al*., 2001). In this test the sample is first bleached to near zero, then given a known laboratory dose thought to be representative of the natural D_e. The SAR protocol is applied to the sample with the first preheat measurement applied after the initial dose administration. Preheat

temperature ranges between 220°C and 260°C are used due to their thermal stability. If the SAR protocol does not yield the applied dose (the dose is not recovered) there is a high probability that the D_e of the natural dose will be inaccurate.

The second test is called the recycling ratio or R-ratio test (Murray & Wintle, 2000). This test is used to check reproducibility (Murray & Wintle, 2000). The R-ratio acts as a simple test to check the reliability of sensitivity corrected dose measurements, i.e. inaccuracies may be detected by the deviated values of these recycled points (Bailey, 2000). Usually two recycled measurements are repeated in the SAR protocol: one with a low dosage to mimic the first regenerative point in which most sensitivity changes take place; and a second with a high dosage. The two recycling ratios $[(L_{x1}/T_{x1})/(L_{x2}/T_{x2})]$ should be very close to unity if appropriate sensitivity corrections during a SAR measurement cycle are applied. In practice less than two standard deviations from unity is acceptable (Murray & Wintle, 2000).

A similar test that was suggested to identify the occurrence of feldspars within a quartz sample (Duller, 2003) is termed the OSL IR depletion ratio test. It is in effect similar to the R-ratio test as it involves two replicate measurements. The first measurement (L_1/T_1) consists of a typical regenerative dose, usually the first regenerative point. The second measurement (L_2/T_2) is a replicate of the first measurement, but before the second measurement the sample is stimulated with infra-red (IR) diodes. As quartz is not affected by IR stimulation, any depletion of the signal measured during L_2/T_2 would be the result of bleaching of any feldspar contamination. A reduction criteria of more than two standard deviations from unity is used to determine an acceptable ratio of $[(L_1/T_1)/(L_2/T_2)]$ (Jacobs *et al.,* 2003a). Anything below this rejection criterion is assumed to be feldspar and is omitted from the analysis. In summary the accuracy of the SAR protocol is tested by a series of prescribed checks. These tests check the validity of the sample by

- Removing and transferring unwanted components of an OSL signal through thermal treatment

- Monitoring the sensitivity of both the Natural signal and regenerated signals (R-ratio)
- Assessing sample contamination.

3.8 D_e Distributions

Single grain analysis demonstrates that relatively few grains contribute to the total luminescence signal obtained from aliquot dating (Jacobs, *in press*). McFee & Tite (1994) relate this to varying levels of dose absorption experienced by individual grains. The single aliquot disc-to-disc scatter experienced by grouping large numbers of grains in aliquots is reduced by averaging out the combined D_e values of many single grains. A good practice is to carry out measurements on a limited grain size fraction and to use size specific masks for each aliquot. Smaller mask sizes result in fewer grains on the aliquot, and the inter-aliquot scatter in OSL measurements may increase because fewer D_e values are averaged. This is not always the case however, and other reasons for scatter could include sample mixing through contamination e.g. roof spall, partially bleached samples and microdosimetry. Microdosimetry relates to grains that lie next to highly radioactive particles such as zircon or the grains themselves could contain radioactive inclusions with higher radioactivity (Wintle, 1997). For these reasons a large number of aliquots are used in D_e determination, 24 in this study, and the D_e values for each aliquot is determined. After aliquots have been rejected using the criteria outlined above the true D_e value is calculated from the combined D_e values of the remaining aliquots.

Correct curve fitting in the dose response analysis allows “true apparent” D_e values to be assessed and any cause of scatter may be a result of other factors mentioned above. In a typical quartz sample the shape of a dose response curve starts to become non-linear as electron traps start to saturate and linear curve fitting may be incorrect in these situations. In this study dose response curves were constructed using regenerative dose points fitted to either an exponential or an exponential plus linear term. This was done by using *Analysis Pro* developed by Geoff Duller. Exponential curve fittings were

used due to the exponential saturation levels experienced in quartz grains (Wintle, 1997). The curves were fitted according to the average error of the fit where the smallest error constituted the best fit. The equation used to describe the term exponential is shown in equation 3.2.

$$I = I_0 + I_{\max}(I - e^{-D/Do}) \qquad \textbf{Equation 3.2}$$

Where:
I is the L_x/T_x ratio,
I_0 indicates the initial part of the luminescence signal,
I_{max} is the upper limit of the luminescence signal,
D is the regenerated laboratory dose,
D_0 is a constant and controls the rate of trap filling.

The equation used for an additional linear term was used when additional traps were created by an administered dose and is shown in equation 3.3

$$I = I_0 + I_{\max}(I - e^{-D/Do}) + k.D \qquad \textbf{Equation 3.3}$$

Where:
k is the additional linear term added to the exponential function represented by a constant.

Once all the D_e values from a specific sample have been acquired, graphic displays may be used to determine whether a single dose population or some other factor evident in overdispersion controls the values of D_e. Two types of plots to represent D_e values are used in this study: a probability density plot (PD plot) and a Radial Plot. The measurement errors obtained through general statistics indicate which type of plot to use.

The PD plots uses each individual D_e values and represents them on a Gaussian curve; the central value is the D_e. The Gaussian curves from the

different grains are summed to create a probability density function. PD plots do not represent true age variation according to measurement precision, whereas radial plots do (Galbraith, 1998). In OSL dating it is preferred to plot D_e estimates with clear reference to their precision (Galbraith, 1990, 1994). Galbraith (1988) suggested the radial plot, where the precisions are clearly plotted on one axis (Figure 3.11). All data on a radial plot is relative to a central value taken as the weighted average by,

$$Z_0 = \left\{ \sum_{i=1}^{n} z_i / \sigma_i^2 \right\} / \left\{ \sum_{i=1}^{n} 1/\sigma_i^2 \right\} \qquad \textbf{Equation 3.4}$$

Where:
Z_0 is the weighted average of all the L_x measurements
Z is the individual L_x measurements and
σ is the standard deviation of each aliquot.

Once the weighted average (WAV) is obtained an x,y scatter plot is constructed. The precision of the sample is displayed on the x axis by $1/\sigma$ and the data points relative to their precision are displayed on the y axis by $(Z-Z_o)/\sigma$. $(Z-Z_o)$ is the slope of the data relative to the WAV (Galbraith, 1990). A third axis, the 'radial axis' represents the individual D_e values from a specific sample. The area in which the data will be represented can be limited by drawing a 2 sigma band around the central value on the y axis. 95% of the points should fall within this band in an ideal sample. When more than 5% of D_e values lie outside the 2 sigma range, the dose distribution is overdispersed. To add a radial or circular scale to the plot, an arc is drawn using a suitable radius and the x, y coordinates are plotted using a suitable reference value by

$$x = r_0 / \left\{ 1 + h^2 (Z - Z_0)^2 \right\}^{12}, \quad y = (Z - Z_0) x \qquad \textbf{Equation 3.5}$$

(Galbraith, 1990)

Where:
r_0 is the radius cantered at x=0, y=0
h is the length of 1 unit of x divided by the length of 1 unit of y

.

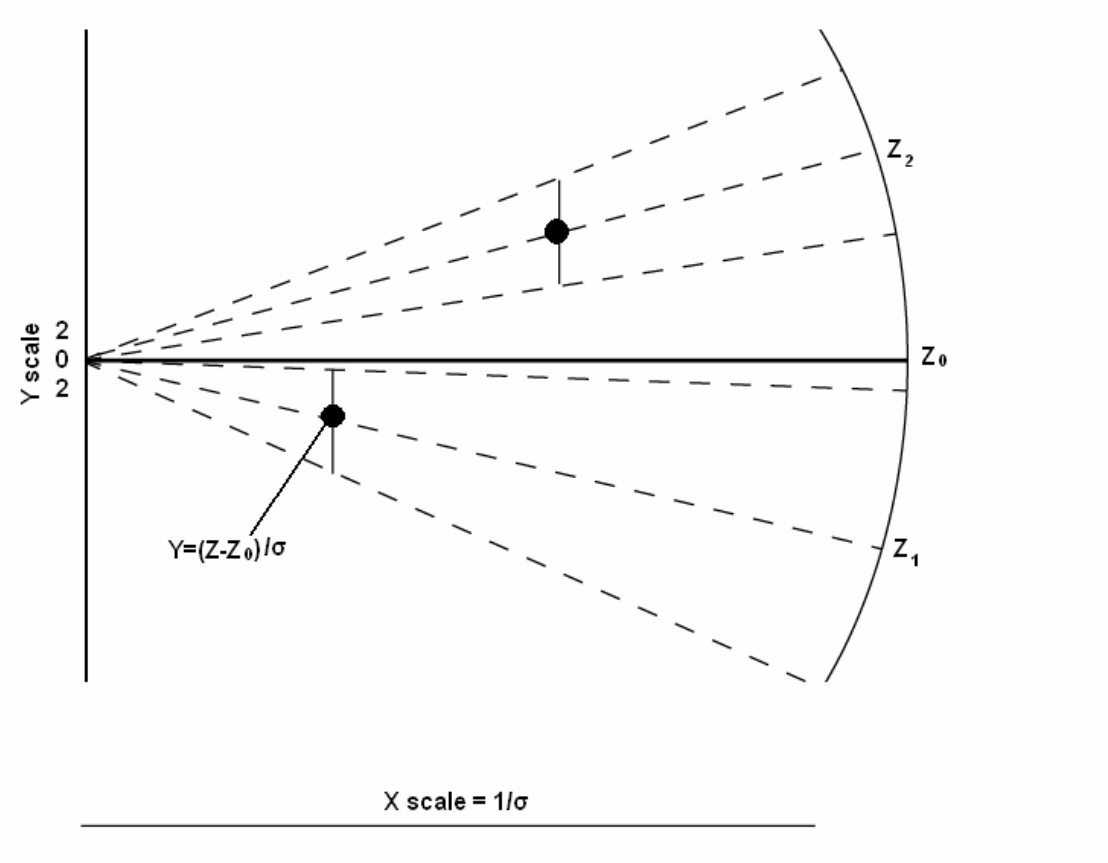

Figure 3.11 General principle of the Radial Plot. Each estimate has a unit standard error on the y scale. Points with larger x i.e. the further to the right points appear the more precise they are. The y values appear on the radial axis and samples that fall within 2 standard deviations from unity are detected on the y axis (Galbraith, 1990).

Overdispersion of D_e values in a radial plot refers to an increased number of data points that lie outside of the two standard deviation bars from a central D_e value (Galbraith *et al.,* 1999). The % overdispersion can be used to determine whether sample mixing has occurred and what type of age model to use in age calculation. Figure 3.12 shows the overdispersion values obtained on a large and small mask size for the same sample.

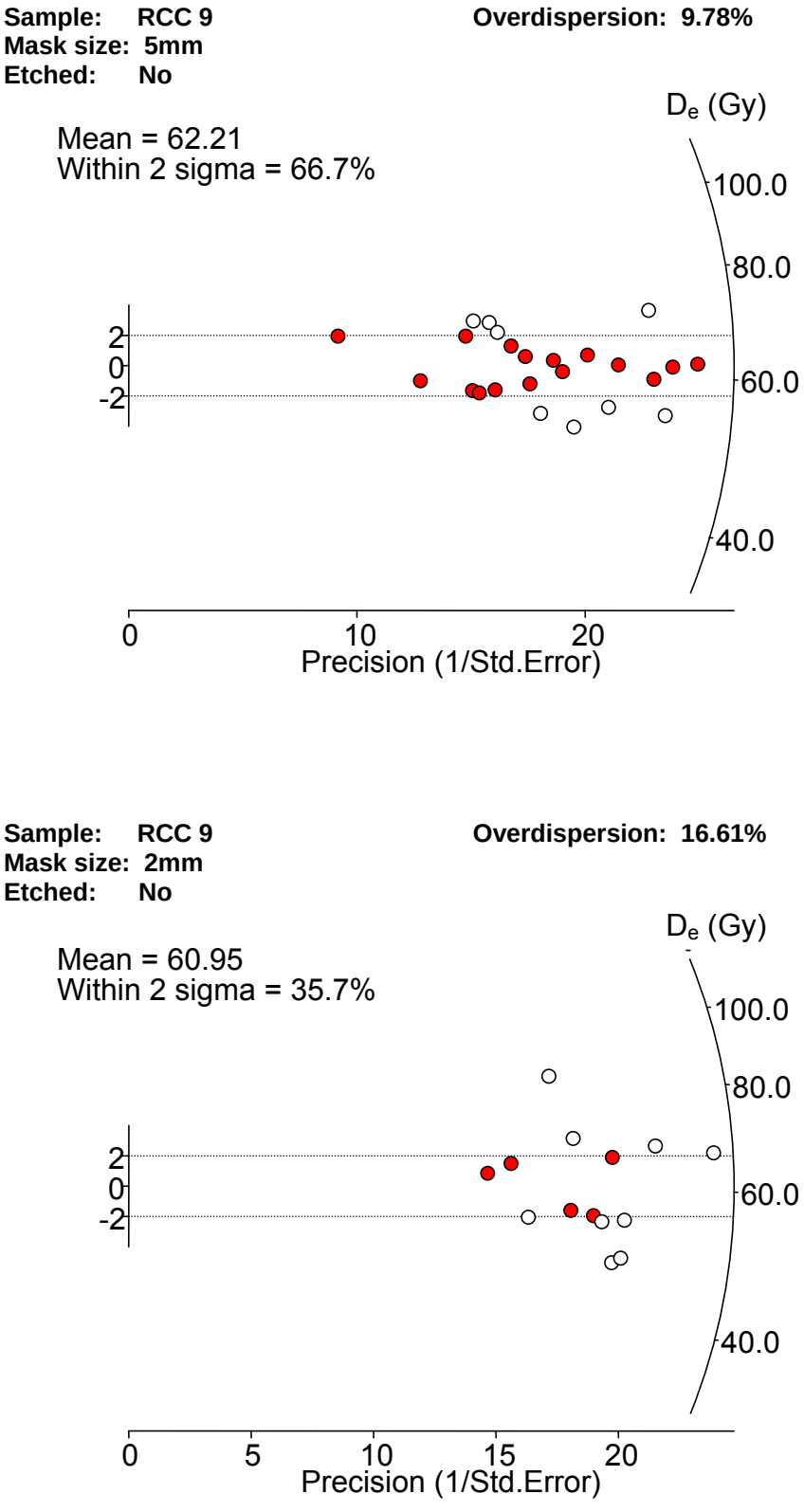

Figure 3.12 Overdispersion values for sample RCC 9 using: a 5mm (top) and 2mm (bottom) mask size.

3.9 Age models

The statistical analysis of D_e values obtained by measuring quartz gives an estimate of the log D_e values and their standard errors. In an ideal sample all aliquots should give consistent estimates of D_e. In some incidences a central estimate of D_e is not the case. Galbraith *et al*. (1999) have suggested the use of three different "age models" that may be used to asses a single D_e value. The models are called the *common age model*, *the central age model* and *the minimum age model*. In the common age model the D_e estimates would be consistent with a common value. If the log D_e values are not consistent with a common value a central age model may be used. In the central age model the D_e values are random and form a normal distribution and the central age can be calculated as the maximum likelihood of the sample. The minimum age model is used to obtain a minimum age of the sample and is used when parameters such as partial bleaching have occurred.

4 OSL DOSIMETRY: THEORY AND EQUIPMENT

4.1 Dose rate determination

The radiation that is relevant to luminescence dating has a broad emission range and is categorized into light and heavy ionizing radiation (Aitken, 1998). It is possible to calculate the overall absorbed radiation dose by assuming a balanced energy system. This implies that the matrix surrounding the sample is greater than the range of the internal radiation. The overall energy absorption is therefore equal to the energy emission. The radiation to which grains are exposed can be divided into an internal and external dose contribution. The internal dose comprises alpha and beta radiation from within the sample grains. The external dose is derived from alpha, beta and gamma radiation from the surrounding matrix, as well as cosmic radiation. The ionising radiation from these elements is provided by daughter isotopes found in radioactive decay chains (see Appendix C). In these chains the half-lives of the isotopes Th, U and K are in the order of 10^9 years, these along with their daughters provide a constant influx of radiation in a soil matrix. Valence electrons in quartz (and other mineral grains in the sediment) absorb this radiation and diffuse into higher energy traps. The result is the accumulation of trapped electrons through time. The rate at which sediments are irradiated during deposition is called the environmental dose rate, and the total absorbed energy is called the equivalent dose (determined in the laboratory as D_e) . The equation used to resolve for time becomes

$$AGE = \frac{EquivalentDose\ (D_E)}{D_\alpha + D_\beta + D_\chi + D_C}$$ (Aitken, 1985; 1998)

Equation 4.1

Where:

$D_\alpha + D_\beta + D_\chi + D_C$ are alpha, beta, gamma and cosmic dose rates.

4.2 Alpha particle contribution

Alpha radiation is less efficient than beta and gamma radiation in the trapping of electrons due to its high ionising density. The alpha particle range is very short and only affects the outer rind of sand-sized grains. Alpha particles consist of 2 neutrons and 2 protons, with 2 units of positive charge ($^{4}_{2}He$) and they are emitted by Th and U (see appendix C). Their contribution is predominantly external in quartz grains, but consideration must be given to the possible inclusion of these elements in quartz. An estimated internal alpha contribution from Th and U for HF etched quartz was calculated to be 0.586 ppm and 0.169 ppm respectively (Jacobs *pers. comm.*). In coarse grain dating (i.e. the quartz inclusion technique developed by Fleming (1966, 1970)) sand-sized grains are selected and etched with 40% Hydrofluoric Acid (HF) typically removing the outer 9µm which is effected by alpha radiation. This has the advantage, if the internal alpha contribution is negligible, of avoiding the need to determine the alpha radiation effectiveness.

If the quartz grains are not etched during laboratory pre-treatment the alpha particle contribution has to be taken into consideration. The alpha particle effectiveness or range that has been affected by alpha radiation for normal sand sized grains is within the range 0.04 to 0.1 mm (Stokes *et al*., 2003), for a 195 µm sized grain the total alpha contribution will be within the 4-12% range (Aitken, 1985). The grain dependant size attenuation of alpha particles in quartz was first calculated by Fleming (1966). Bell (1980) later calculated the alpha attenuation in grain sizes ranging from 1 µm to 1mm showing alpha penetration in fine grains to be < 90% of the total grain. Figure 4.1 shows that the average alpha dose received by grains in the diameter of 195 µm is below 20%.

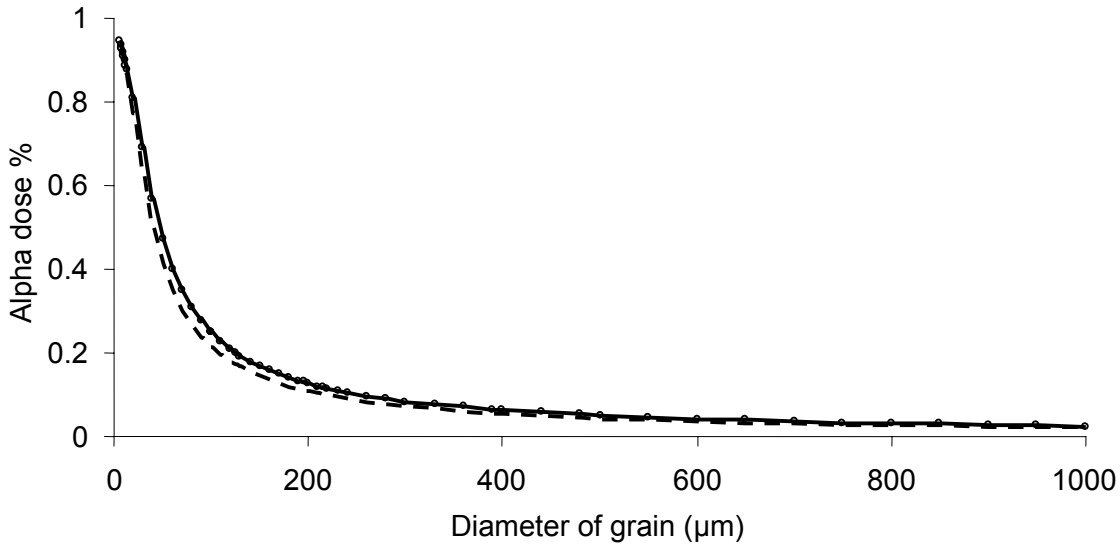

Figure 4. 1 Average alpha dose for quartz grains embedded in a matrix that contains thorium and uranium (after Bell, 1980). The dashed line represents the alpha contribution from Th, the solid line represents the alpha contribution from U. The attenuation factor is derived for uranium using a linear regression formula of 19.602 × grain size$^{-0.9811}$ and for thorium 22.701 × grain size$^{-0.9802}$.

Two factors affect the absorption of alpha radiation. First, the alpha absorption coefficient is proportional to the effective track length, as the energy loss of the alpha particle increases per unit length as the particle slows down (Aitken, 1985). Second, the moisture in the soil matrix attenuates the alpha contribution. The moisture content of a sample can vary from 1% to 40%, the upper limit being the saturation level (Aitken, 1985). The alpha particle contribution for samples from RCC was calculated using an alpha effectiveness of 0.04, and attenuation factors for un-etched material was taken into account using values obtained from figure 4.1. The dry alpha dose rates were also corrected for moisture content using equation 4.2 (Aitken, 1985).

$$D_{\alpha} = \frac{D_{\alpha,dry}}{1+1.50WF} \qquad \text{Equation 4.4 (Aitken, 1985)}$$

Where:

D_{α} is the effective 'dry' alpha dose rate.

W is the saturated moisture content of the sample (expressed as the ratio between the weight of "wet" sample and the weight of sample after it has been dried).
F is the average level of saturation over the sample's burial period.

4.3 Beta, gamma and cosmic radiation

The beta and gamma radiation relevant to luminescence dating are emitted by K, U, Th and a small contribution from Rb. They have longer ionising ranges and any absorbed dose is predominantly from an external source. In soil beta particles have a typical range of 2mm, gammas roughly an order of magnitude higher than beta's, and cosmic radiation can reach a few metres into the soil (figure 4.3) (Aitken, 1985). The overall environmental dose rate consists of roughly two thirds beta irradiation (Mejdahl, 1979) (see figure 4.2). Gamma rays are the second largest contributors to the dose-rate. Gamma rays from the decay of ^{40}K also make a small contribution to the internal dose of a grain. Self dose percentage is used as a concept to describe the internal gamma dose rate and constitutes a small percent of the total gamma dose rate (see figure 4.4). The equation for the D_γ component becomes:

$$D_\gamma = \frac{p}{100} D_\gamma^i + \left(1 - \frac{p}{100}\right) D_\gamma^e \quad \text{(Aitken, 1985)}$$

Equation 4.3

Where:
P is the average gamma dose in the sample (expressed as a percentage),
D_γ^i and D_γ^e are the internal and external gamma dose rates.

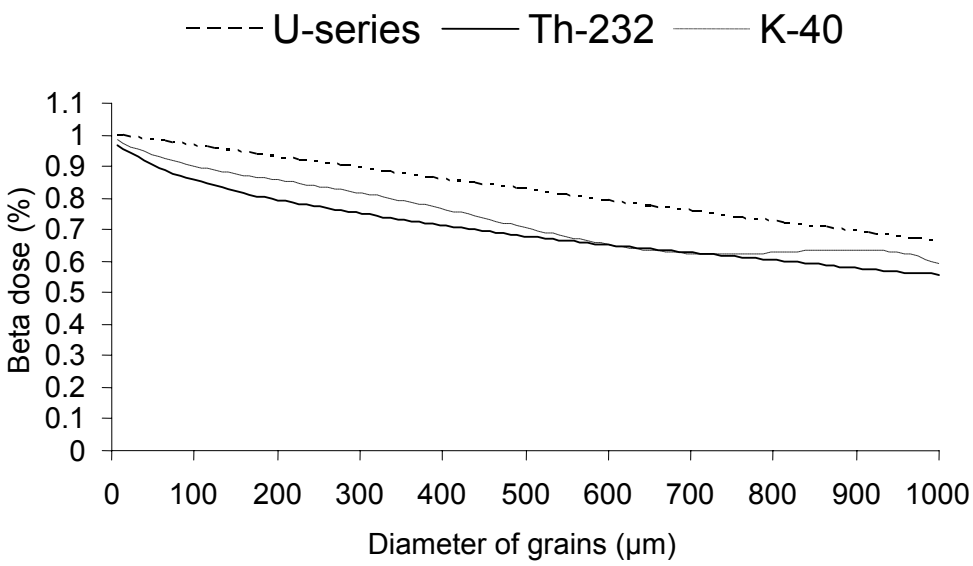

Figure 4. 2 Average beta dose from surrounding matrix to spherical grains (after Mejdahl, 1979).

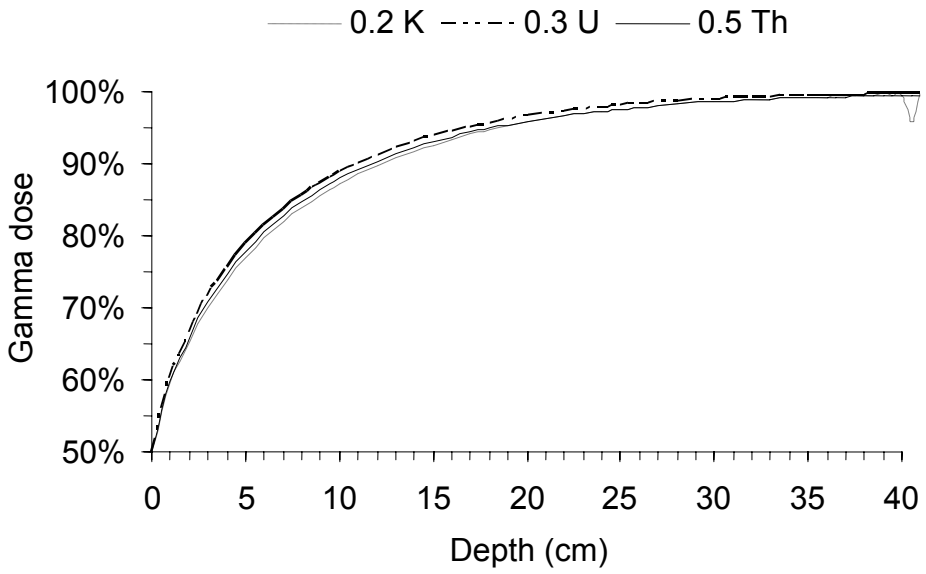

Figure 4. 3 Variation of gamma dose in soil, expressed as a % of the gamma dose at infinite depth (from computation by Løvborg in Aitken, 1985).

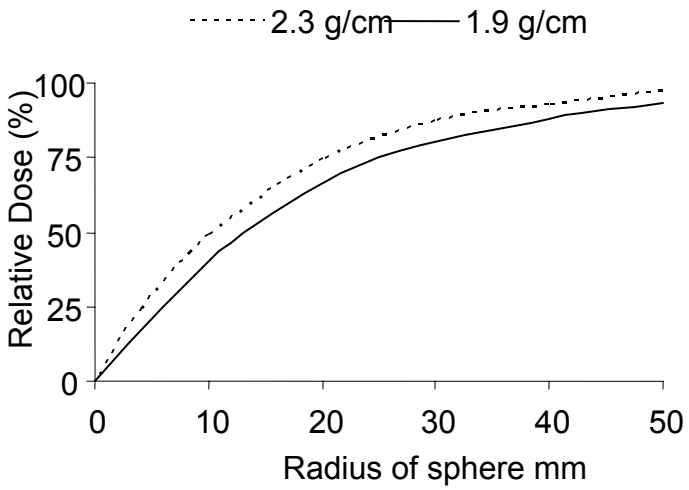

Figure 4. 4 Self dose at the centre of a sphere for gamma radiation with energy 2MeV (from Aitken, 1985).

The cosmic ray contribution constitutes a small fraction of the total environmental dose rate. The value used to define the cosmic ray contribution needs to be adjusted for overburden and altitude (Aitken, 1985). Cosmic rays are made up of 'soft' and 'hard' components. The soft component, consisting mostly of electrons, is absorbed by the first half metre of soil. The hard component, also used in assessing the dose rate, comprising mostly of muons (Aitken, 1985). The muons can be observed with decreasing intensity at substantial depths (Prescott & Hutton, 1994) (Figure 4.5). The cosmic contribution to the dose rate is also affected by latitude and altitude.

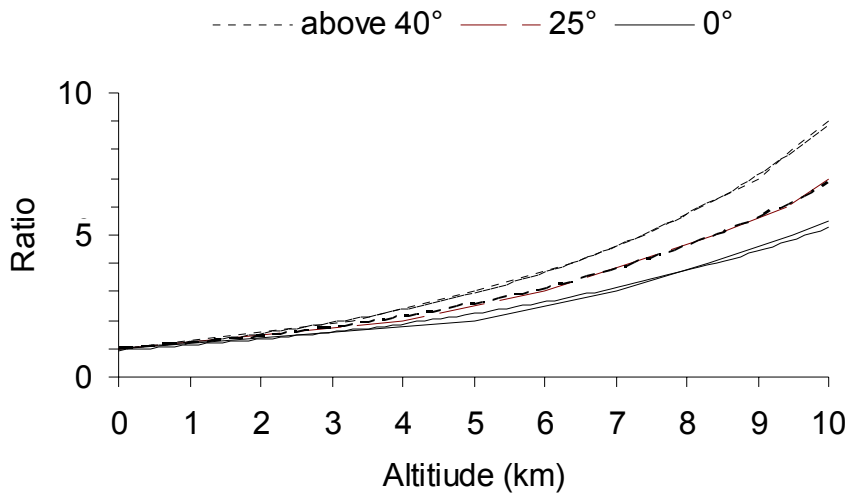

Figure 4. 5 Variation of the intensity of cosmic rays with altitude, expressed as a ratio for which the corresponding annual dose is 185 µGy/a (from Aitken, 1985).

The dry dose rates from beta particles and gamma rays must also be corrected for moisture attenuation unless in situ gamma measurements are performed. The moisture content correction is made in terms of *WF*, where:

W=(saturation wet weight-dry weight) / (dry weight)
F=(average water content) / (saturation water content) (Aitken, 1985).

The value used for *F* is usually estimated and is expressed as a fraction of the saturated water content. It has also been estimated (Zimmerman, 1971) that the absorption coefficient is 50% higher for alpha radiation, 25% for beta radiation and 14% for gamma radiation. Then to obtain the true or 'Wet' dose rates the actual values are given by

$$D_{\beta} = \frac{D_{\beta,dry}}{1+1.25WF}$$
$$D_{\gamma} = \frac{D_{\gamma,dry}}{1+1.14WF}$$

Equations 4.3

4.4 Instrumentation used to determine dose rates

Dose rates were determined by Thick Source Alpha Counting (TSAC) combined with X-ray Fluorescence measures of K as well as *in situ* gamma measurements. Alpha counting was done using a Daybreak 583 thick source alpha counter. TSAC measures paired activity of U and Th assuming that all the daughters are present in equilibrium. The instrument has a 0.02 to 0.4 s window in which it is able to measure `slow pairs`. Slow pairs reflect the decay of ^{216}Po (half-life 0.145 s) into ^{212}Pb in the Th chain (see appendix C). By factoring the probability of detecting a slow pair, the pairs count can be used to calculate the contribution of the Th chain to the total alpha count. The remaining alpha counts are presumed to derive from the U chain (Aitken, 1985).

The samples are measured in a 42mm diameter holder (area = 1385 mm^2). The sample holder contains a zinc sulphide (ZnS) screen that produces scintillations when struck by alpha particles. The scintillation events can be measured accurately with modern photomultiplier tubes (Aitken, 1985). The output from the daybreak TSAC is in the form of raw ppm concentrations of U and Th, but the output values could not be replicated manually using the standard approach. In this study the values were calculated using the raw counts (see appendix C).

Determination of the external dose rate can be problematic due to the heterogeneity of the sample matrix. A solution to the problem is to measure the gamma radiation contribution *in situ* using a portable gamma spectrometer. This method is relatively fast but has the disadvantage of having to auger a hole in the sample site that is wider than the detector and at least 30 cm in depth. For archaeologically sensitive sites, such as RCC, the auger hole could overlap the desired layer, as well as destroy site information. When using a portable gamma spectrometer, the individual dose rate contributions from Th, U and K are determined (Aitken, 1985). The spectrometer used in this study was an Aptec portable gamma spectrometer with a 2 inch NaI crystal, doped with thallium (Tl) as an activator. Scintillations produced by gamma rays are measured by a photomultiplier tube (one pulse per gamma ray) and produces a corresponding electrical pulse. The electron has the same energy as the gamma photon and dissipates its energy in the crystal (Aitken, 1985). Figure 4.6 taken from sample RCC 10 shows the spectrum from a typical RCC soil sample.

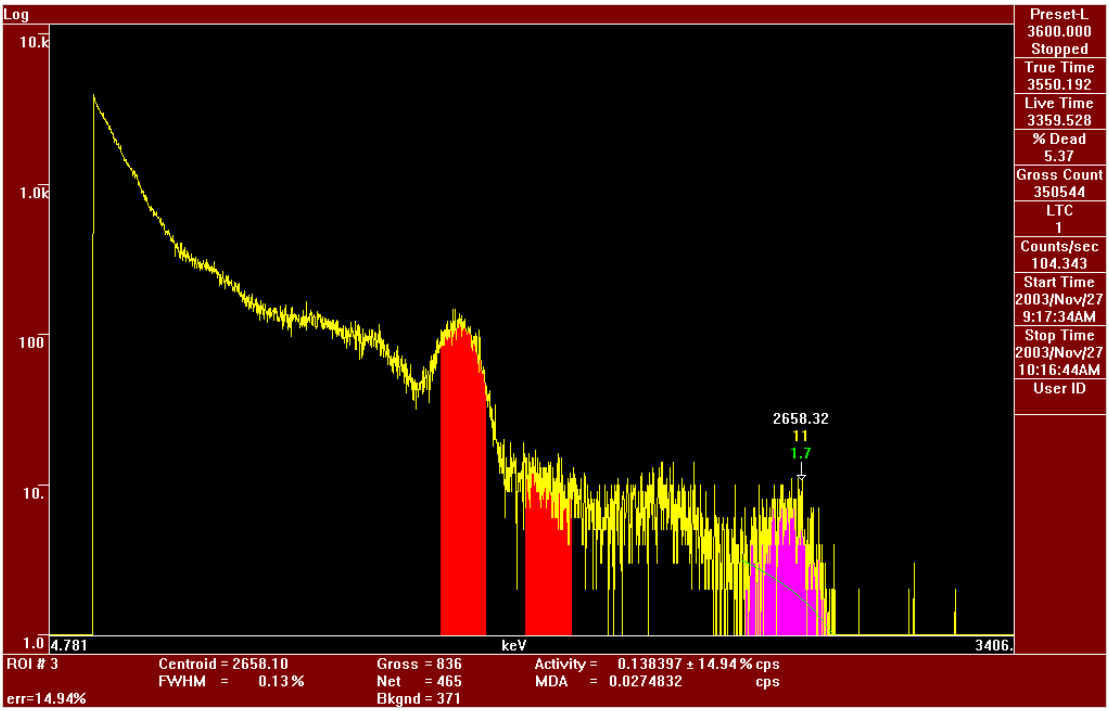

Figure 4. 6 Spectrum derived from a portable gamma spectrometer showing the energy range or photopeaks for the main radioactive elements used in luminescence dating.

With the gamma spectrometer used in this study a full spectrum of gamma radiation pulses are measured, and an acceptance 'window' is generated centred on the range of pulse heights concerned with each radioactive peak (Aitken, 1985). For ^{40}K the peak is 1.46 MeV and the corresponding integration is between 1.38 and 1.53 MeV. For uranium the peak is 1.76 MeV, and is integrated between 1.69 and 1.84 MeV, and for thorium the peak is at 2.61 MeV and is integrated between 2.46 and 2.76 MeV. The system was calibrated using the calibration blocks at Oxford University, and the same integration windows were used.

In order to obtain acceptable precision on the detection counts, the field measurements were conducted for a minimum of 40 minutes, but where time allowed a minimum of 60 minutes was used. Multiple peak identification was used to calibrate the energy scale of the spectrometer and to compensate for any drift that may occur during field measurements.

4.5 Calculation of dose-rates

The dose rates derived in this thesis are from the measurement of element concentrations (ppm) by means of conversion factors calculated by Adamiec & Aitken (1998). The 'Dry dose rates' expressed as a direct conversion from elemental concentration to dose rates need to be corrected for attenuation controlled by moisture content and the effective alpha particle contribution. The conversion factors taken from Adamiec & Aitken (1998) are shown in table 4.1

Table 4.1 Conversion factors used for dose rate calculation (Adamiec & Aitken, 1998).

	^{232}TH	^{238}U	^{235}U	Natural U	^{40}K
Abundance by weight	100%	99.29%	0.71%	-	-
Half-life	14.05	4.468	0.704	-	1.277
Parent activity (Bq/mg)	4.06	12.4	80	12.9	
Dose-rate (Gy/ka) per ppm					
Alpha, full series	0.732	2.685	16.6	2.78	0
Beta, full series	0.0273	0.143	0.515	0.146	0.782
Gamma, full series	0.0476	0.112	0.269	0.113	0.243

Dry dose rates were corrected for attenuation affects on grain size, then by the effects of moisture. Values used for the two grain sizes used for analysis are given in table 4.2 below.

Table 4.2 External attenuation factors

	Average grain Size	
Alpha attenuation	**126µm**	**195µm**
Th	0.199	0.130
U	0.171	0.111
Beta attenuation		
Th	0.891	0.856
U	0.838	0.797
K	0.955	0.932

4.5.1 Dose-rate calculation – A worked example

The calculations are taken from data obtained for sample RCC 10 shown in table 4.3. The example below was chosen as it comprises alpha attenuation calculations, for etched samples this step was simply ignored.

Table 4.3 Raw data for sample RCC 10

	Raw data	**Error**
^{232}Th ppm	3.4264	0.3889
^{238}U ppm	1.2551	0.0413
K%	1.45	
Cosmic contribution	60	20
Moisture content	10	2
Grain size (μm)	195	
Alpha efficiency	0.04	0.02

The Th, U and K concentrations are multiplied by their corresponding conversion factors given in table C1 to obtain the 'Dry dose rate (Gy/ka)', and then corrected for grain size attenuation using values taken from table 4.2 See table 4.4 below.

Table 4.4 Dry dose rates (Gy/ka) for sample RCC 10

	Alphas	**Betas**	**Gammas**
Th	2.508 ± 0.285	0.094 ± 0.011	0.163 ± 0.019
U	3.489 ± 0.115	0.183 ± 0.006	0.142 ± 0.005
K		1.134	0.352
Corrected for grain size attenuation			
Th	0.324 ± 0.037	0.080 ± 0.009	.0163 ± 0.019
U	0.387 ± 0.013	1.146 ± 0.005	0.142 ± 0.005
K		1.058	0.352

The dry dose rates are added together and corrected for moisture content however, the alpha contribution from Th and U needs to first be corrected by the alpha efficiency factor of 0.04. The dry dose rate then becomes,

Alpha:	0.028 ± 0.002	
Beta:	1.284 ± 0.014	
Gamma:	0.657 ± 0.023	Example 4.1

The ‘wet’ dose-rates or true dose rates become:

Alpha:	0.024 ± 0.002	
Beta:	1.126 ± 0.014	
Gamma:	0.583 ± 0.023	
Total dose-rate:	**1793.25 ± 38.25 Gy/Ka**	Example 4.2